

Rochester Institute of Technology

RIT Digital Institutional Repository

Theses

5-2-2019

Aerospace Fuel Flow Metering Check Valve Model, Simulation, and Validation

Trevor M. Crandell
tmc2758@rit.edu

Follow this and additional works at: <https://repository.rit.edu/theses>

Recommended Citation

Crandell, Trevor M., "Aerospace Fuel Flow Metering Check Valve Model, Simulation, and Validation" (2019). Thesis. Rochester Institute of Technology. Accessed from

This Thesis is brought to you for free and open access by the RIT Libraries. For more information, please contact repository@rit.edu.

Aerospace Fuel Flow Metering Check Valve Model, Simulation, and Validation

Submitted by:
Trevor M. Crandell

A Thesis Submitted in Partial Fulfillment of the Requirements for the Degree of
Master of Science in Mechanical Engineering

Rochester Institute of Technology
Rochester, NY
Department of Mechanical Engineering
Kate Gleason College of Engineering
May 2, 2019

Approved by:

Dr. Jason Kolodziej _____
Associate Professor, Department of Mechanical Engineering(Thesis Advisor)

Dr. Michael Schrlau _____
Associate Professor, Department of Mechanical Engineering

Dr. Mario Gomes _____
Senior Lecturer, Department of Mechanical Engineering

Dr. Steven Day _____
Department Head, Department of Biomedical Engineering

Permission to Reproduce

I, Trevor M Crandell, hereby grant permission to the Wallace Memorial Library of Rochester Institute of Technology to reproduce my thesis in the whole or in part. Any reproduction will not be for commercial use or for profit.

May, 2019

Acknowledgements

I'd like to acknowledge and give thanks to all my friends, family, and peers who contributed to the completion of this work.

Specifically, I'd like to thank my advisor, Dr. Kolodziej for taking on my thesis topic even though it was outside his normal field of research and helping make sure I stayed on track.

Additionally, I'd like to thank Advanced Atomization Technologies and Rochester Institute of Technology for providing the resources for this project. All equipment resources were provided by Advanced Atomization Technologies. I appreciate and thank both Rochester Institute of Technology and Advanced Atomization Technologies for their financial support of this project.

Finally, I'd like to thank my parents, Michael and Katrina Crandell for providing me with motivation, support, focus, and the work ethic to see this project through to the end.

Abstract

The fuel atomizer of a gas turbine engine is a critical component of study, design, and manufacture for the gas turbine industry. Modern engines rely on consistent precise operation of fuel nozzles to achieve today's progressive emission standards and to keep engines operating longer and to keep them overall more competitive. The previous research into this field is extensive but has left a gap where relatively computationally simple methods can be used to benefit companies that build aerospace fuel nozzles. Through simulation and experimentation, the goal of this research was to create a method of modeling aerospace fuel nozzle flow metering valves that is less computationally intense than complex CFD and generates high resolution information for the design and manufacture of said valves. A system was developed in MATLAB and Simulink with the intent of matching the valve system and its outputs to an experimental setup. This paper primarily evaluates the simulation methods' accuracy, experimental methods used and the use of cost analysis for optimization. Through experimentation and simulation optimization a relatively accurate simulated system is generated that matches valve stroke and flow output relatively well. Cost analysis optimization methods failed to establish accurate results and several theories as to why this happened were generated and discussed.

Table of Contents

Permission to Reproduce.....	i
Acknowledgements.....	ii
Abstract.....	iii
Table of Contents.....	iv
Figures List.....	vi
Tables List.....	xii
Nomenclature List.....	xiii
1. Introduction.....	1
1.1 Valve Design in Aerospace Fuel Nozzles.....	2
1.2 Challenges in Design and Manufacturing.....	3
2. Prior Work Review.....	3
2.1 Steady State Valve Simulation.....	3
2.2 CFD Modeling Approaches.....	4
2.3 Valve Coefficient Studies.....	6
2.4 Condition Monitoring of Check Valves.....	7
2.5 Vibration Analysis of Fluid Containing Systems.....	7
3. Research Gap.....	9
4. Methods.....	9
4.1 Defining Boundaries of the Model.....	9
4.2 Forces Acting on Valves.....	10
4.3 Mass-Spring-Damper System.....	11
4.4 Simulink Simulation.....	12
4.5 Flow Area Calculations.....	14
4.6 Experimental System Setup.....	19
4.7 Experimental Data Collection Plan.....	24
4.8 Model Optimization Technique.....	26
5. Results.....	27
5.1 Experimental and Empirical Data Collection.....	27
5.2 Simulation.....	34
5.3 Cost Analysis Optimization with Transient Data.....	36
5.4 Manual Optimization.....	39

5.5	Cost Analysis Optimization with Steady State Data.....	47
5.6	Uncertainty Analysis	49
5.7	Further Research Opportunities	56
6.	Conclusions	57
7.	Bibliography	58

Figures List

Figure Number	Description of Figure	Page Number
1	CFM56 Fuel Nozzle Cross-Section with Flow Paths. This cross section image was provided by Advanced Atomization Technologies.	1
2	Check valve symbol and types: (a) ball valve, (b) poppet valve, (c) plate valve, and (d) multidisk plate valve [2]	2
3	Simplified poppet valve diagram [2]	2
4	Example of specialized flow slot geometry Simplified poppet valve diagram [2]	2
5	Cross-section of hydraulic flow control check valve studied by H. Xie, J. Liu, H. Yang and X. Fu [1]	3
6	Cross-section of reed style check valve studied by A. L. Knutson [2]	4
7	Cross-section of a pressure regulation valve studied by B. K. Saha, H. Chattopadhyay, P. B. Mandal and T. Gangopadhyay [3] and H. Chattopadhyay, A. Kundu, B. K. Saha and T. Gangopadhyay [4]	4
8	Cross-section of a hydraulic control valve studied by E. Frosina, A. Senatore, D. Buono and K. A. Stelson [5]	5
9	Geometry of the flow slots of a hydraulic control valve for construction equipment studied by Y. Ye, C.-B. Yin, X.-D. Li, W.-j. Zhou and F.-f. Yuan [6]	5
10	Images of hydraulic control valve design configurations investigated by E. Lisowski and G. Filo [7]	6
11	Image of the check valve used in the study by E. Leati, C. Gradl and R. Scheidl [8]	6
12	Cross-section of swing style check valve studied by M.-R. Lee, J.-H. Lee and J.-T. Kim [9]	7
13	Diagram of the liquid filled pipe systems studied by Q. S. Li, K. Yang, L. Zhang and N. Zhang [10]	8
14	3D model of the pipe system studied by P. Persson, K. Persson and G. Sandberg [11]	8
15	Cross-section the orifice and pipe studied by J. Herrmann, J. Koreck, M. Maess, L. Gaul and O. v. Estorff [12]	8

16	Cross section of CFM56 with focus on valve housing area.	9
17	Simplified representation of the check valve for the primary circuit.	10
18	Simplified representation of the flow divider valve for the secondary circuit.	10
19	Free body diagrams showing 3 configurations of valve actuation. A closed valve(left), partially open valve(middle) and fully open valve(left) are shown. X represents direction of positive force and valve actuation direction	11
20	Simulink model of a mass spring damper system with a step input and an output of displacement. Similar to the thesis research model.	12
21	Simulink model of the Flow Divider Valve.	13
22	Simulink model of the Check Valve	13
23	Comparison of area affected by pressure differential across valve in closed and open state. Highlighted yellow area indicates area of pressure affect. Blue arrows represent fluid flow. Left valve is open and right valve is closed.	14
24	Cross section of flow divider valve in the fully closed position. Image taken from 3D model of the FDV.	16
25	Cross section of flow divider valve in the fully closed position from an isometric viewing angle to provide further perspective of the flow slot. Image taken from 3D model of the FDV.	16
26	Cross section of flow divider valve flow area during clearance only leakage flow.	17
27	Cross section of flow divider valve flow area during flow slot flow opening.	17
28	Flow slot area for flow divider valve with stroke increased linearly. Time used instead of stroke for intellectual property reasons.	18
29	Cross section of check valve flow area.	19
30	References for area between valve seat and poppet.	19
31	Simplified diagram of the experimental system used for data acquisition.	21
32	FDV fixturing for fluid pressure and laser displacement measurement and data collection. Made out of acrylic.	22
33	CV fixturing for fluid pressure and laser displacement measurement and data collection. Made out of acrylic.	22
34	Mirror surface in the assembled CV.	23
35	Mirror surface on poppet out of assembly.	23

36	FDV with mirror glued to spool in assembly.	23
37	Mirror glued to spool out of assembly.	23
38	Data plot of optical sensor calibration with linear best fit line	28
39	FDV during data collection. Shows test pressure point with no cavitation/bubble formation.	29
40	FDV during data collection. Shows test pressure point with cavitation/bubble formation.	29
41	All FDV's stroke data collected from the High Impulse Testing program	31
42	All FDV's stroke data collected from the Continuous Step Increase program.	31
43	All FDV's flow data collected with test stand from the High Impulse Testing program.	32
44	All FDV's flow data collected with test stand from the Continuous Step Testing program.	33
45	Plot comparing all valves stroke response with the only variables being the empirically collected measurements of the valves. Simple pressure signal input used in Simulink.	34
46	Plot comparing all valves flow with the only variables being the empirically collected measurements of the valves. Simple pressure signal input used in Simulink.	34
47	CV simulated stroke results with near production test points.	35
48	CV simulated flow results with near production test points.	35
49	Cost Value of an optimization attempt made on Valve 7 simulation, Continuous Step Increase program.	36
50	Valve 5 simulation with cost analysis optimized values	37
51	Valve 6 simulation with cost analysis optimized values	37
52	Valve 7 simulation with cost analysis optimized values	37
53	Valve 8 simulation with cost analysis optimized values	37
54	Valve 9 simulation with cost analysis optimized values	38
55	Plot showing the effects of varying the pressure area variable on the stroke of Valve 7	39
56	Plot showing the effects of varying the damping ratio variable on the stroke of Valve 7.	40

57	Plot showing the effects of varying the spring preload variable on the stroke of Valve 7.	40
58	Valve 5 simulation manually corrected to match reality	41
59	Valve 5 corrected variables compared to other program	41
60	Valve 6 simulation manually corrected to match reality	41
61	Valve 6 corrected variables compared to other program	41
62	Valve 7 simulation manually corrected to match reality	42
63	Valve 7 corrected variables compared to other program	42
64	Valve 8 simulation manually corrected to match reality	42
65	Valve 8 corrected variables compared to other program	42
66	Valve 9 simulation manually corrected to match reality	42
67	Valve 9 corrected variables compared to other program	42
68	Plot showing the effects of varying the coefficient of discharge variable on the flow of Valve 7.	43
69	Plot showing the effects of varying eccentricity variable on the flow of Valve 7.	44
70	Valve 5 simulation manually corrected to match reality	45
71	Valve 5 corrected variables compared to other program	45
72	Valve 6 simulation manually corrected to match reality	45
73	Valve 6 corrected variables compared to other program	45
74	Valve 7 simulation manually corrected to match reality	45
75	Valve 7 corrected variables compared to other program	45
76	Valve 8 simulation manually corrected to match reality	46
77	Valve 8 corrected variables compared to other program	46
78	Valve 9 simulation manually corrected to match reality	46
79	Valve 9 corrected variables compared to other program	46
80	Plot of the cost value of each iteration of the "fminsearch" optimization	48
81	Valve 5 simulation with cost analysis optimized values	48
82	Valve 6 simulation with cost analysis optimized values	48

83	Valve 7 simulation with cost analysis optimized values	49
84	Valve 8 simulation with cost analysis optimized values	49
85	Valve 9 simulation with cost analysis optimized values	49
86	Valve 5 High Impulse Test Program stroke	50
87	Valve 5 Continuous Step Test Program stroke	50
88	Valve 6 High Impulse Test Program stroke	51
89	Valve 6 Continuous Step Test Program stroke	51
90	Valve 7 High Impulse Test Program stroke	51
91	Valve 7 Continuous Step Test Program stroke	51
92	Valve 8 High Impulse Test Program stroke	51
93	Valve 8 Continuous Step Test Program stroke	51
94	Valve 9 High Impulse Test Program stroke	52
95	Valve 9 Continuous Step Test Program stroke	52
96	Valve 5 Continuous Step Test Program flow	52
97	Valve 5 High Impulse Test Program flow	52
98	Valve 6 Continuous Step Test Program flow	52
99	Valve 6 High Impulse Test Program flow	52
100	Valve 7 Continuous Step Test Program flow	53
101	Valve 7 High Impulse Test Program flow	53
102	Valve 8 Continuous Step Test Program flow	53
103	Valve 8 High Impulse Test Program flow	53
104	Valve 9 Continuous Step Test Program flow	53
105	Valve 9 High Impulse Test Program flow	53
106	Unprocessed(raw) empirical data of the FDV stroke showing the effects of cavitation.	54
107	Close up of the simulation of the valve stroke matching well with reality in terms of damped reaction in Valve 6	55

108	Close up of the simulation of the valve stroke of valve 6 failing to match empirical data due to what appears to be cavitation/bubble interference in the experimental data optical sensor reading.	56
-----	-----------------------------------------------------------------------------------------------------------------------------------------------------------------------------------------------------	----

Tables List

Table Number	Description	Page Number Location
1	Valve Testing Equipment	20
2	Testing Profiles for FDV	25
3	Testing Profiles for CV	26
4	FN for FDV Fixturing	28
5	Cost Analysis Optimized Results	36
6	Manually Optimized Results	46
7	Steady State Cost Analysis Optimization of Stroke	47
8	Sensor Error Data Summary	49

Nomenclature List

AATech	Advanced Atomization Technologies
RIT	Rochester Institute of Technology
Cal. Fluid	MIL-PRF-7024 Type II
FDV	Flow Divider Valve – Secondary Flow
CV	Check Valve – Primary Flow
CV1	Control Volume 1 – Upstream of CV
CV2	Control Volume 2 – Fluid in CV, between press. taps
CV3	Control Volume 3 – Downstream of CV
CV4	Control Volume 4 – Upstream of FDV
CV5	Control Volume 5 – Fluid in FDV, between press. taps
CV6	Control Volume 6 – Downstream of FDV
A_2	Flow area through CV
x_p	Stroke of CV
A_4	Flow area through FDV
x_s	Stroke of FDV
P_{ip}	Pressure at inlet of CV system
W_{ip}	Flow rate at inlet of CV system
A_{ip}	Flow area at inlet of CV system
mdot_p	Mass flow rate at inlet of CV system
P1	Pressure at upstream press. tap for CV system
A1	Area at upstream press. tap location for CV system
P2	Pressure at downstream press. tap for CV system
Pop	Pressure at outlet of CV system(atmospheric press.)
Aop	Area at outlet of CV system
Pis	Pressure at inlet of FDV system
Wis	Flow rate at inlet of FDV system

A_{is}	Flow area at inlet of FDV system
\dot{m}	Mass flow rate at inlet of FDV system
P₃	Pressure at upstream press. tap for FDV system
A₃	Area at upstream press. tap location for FDV system
P₄	Pressure at downstream press. tap for FDV system
P_{os}	Pressure at outlet of FDV system(atmospheric press.)
A_{os}	Area at outlet of FDV system
<i>F</i>	Sum of forces acting on valves
<i>F_p</i>	Force of pressure differential
<i>F_{spr}</i>	Force of spring
<i>F_{seat}</i>	Force from valve seat
<i>k_{spr}</i>	Spring constant
<i>x_{preload}</i>	Spring preload displacement
<i>x_{max}</i>	Max displacement of spring
<i>P_u</i>	Upstream pressure
<i>A_u</i>	Upstream area
<i>P_d</i>	Downstream pressure
<i>A_d</i>	Downstream area
ζ	Damping ratio
ω_0	Undamped natural frequency
<i>c</i>	Damping coefficient
<i>k</i>	Spring constant
<i>M</i>	Total mass of system
<i>M_{spool}</i>	Mass of spool
<i>M_{spring}</i>	Mass of spring
<i>A_{cv}</i>	Check valve flow area
<i>R₁</i>	Variable in check valve flow area, see Fig. 12
<i>R₂</i>	Variable in check valve flow area, see Fig. 12

h	Variable in check valve flow area, see Fig. 12
θ	Variable in check valve flow area, see Fig. 12
X	Variable in check valve flow area, see Fig. 12
FN	Flow number
W_f	Flow rate
ΔP	Pressure drop across valve
A	Flow area
C_d	Coefficient of discharge
S	Specific gravity of fluid
W_{fbleed}	Bleed flow rate
ρ	Density of fluid
r	Radius of spool
C_r	Radial clearance of spool
μ	Absolute viscosity of fluid
L	Length of bleed
e	Eccentricity of shaft to the bore
e_{bleed}	Eccentricity simplified constant
A_{cv}	Area of check valve flow
R_1	Radius 1 in Fig. 23
R_2	Radius 2 in Fig. 23
h	Height in Fig. 23
X	Geometric measurement in Fig. 23
θ	Angle of flow passage in CV
Dewesoft	Data acquisition device brand name
CFD	Computational Fluid Dynamics
PPH	Mass flow rate in Pounds per hour (English)
MATLAB	Numerical computational environment produced by MathWorks
Simulink	Graphical programming environment for modeling and simulating

1. Introduction

Modern gas turbine combustion and the gas turbine industry derives much of its improvements from control of combustion dynamics through combustion zone study. One primary component of the combustion zone of a gas turbine is the atomizer which provides atomized fuel flow to the combustor for an efficient and clean burn. Without the proper air to fuel ratio and a well atomized fuel source, clean gas turbine fuel burn is not practically possible. To achieve cleaner burns and reach the edge of combustor zone science capability, the fuel delivery into the combustor must be understood and improved. Fluid flow is delivered through meticulously designed and manufactured fuel nozzles to achieve the needs of the combustor zone.

There has been a substantial amount of work done on the modeling of fluid delivery to combustor zones. Most academic work on the subject is focused on the complex fluid dynamics at the outlet of the fuel nozzle. This dynamic is a high priority to researchers as it has the greatest direct impact on emissions and overall function of the combustion of the gas turbine engine. Describing what dynamic is necessary at the outlet of the fuel nozzle is more valuable in the sense that it impacts a broader range of application in the field of combustors, while predicting internal flow behavior is critical to the designer and manufacturer of the fuel nozzles. Also, there is a wider depth of options for delivering flow through a fuel nozzle to the atomizer and each fuel nozzle manufacturing company would have unique methods to deliver that fuel. This coupled with the fact that each fuel nozzle has unique shapes for engine fit and unique fluid flow profiles makes it hard to generalize research on the flow in the fuel nozzle. Research on the fluid flow through fuel nozzles seems to be mostly limited to within company intellectual property(IP) due to these coupled reasons. This is expected, but leaves a gap in available research on tools to describe the flow through an aerospace fuel nozzle. Fig. 1 shows an image of the cross section and flow paths that are the subject of the thesis research. This is the fuel nozzle and two valves that were modeled.

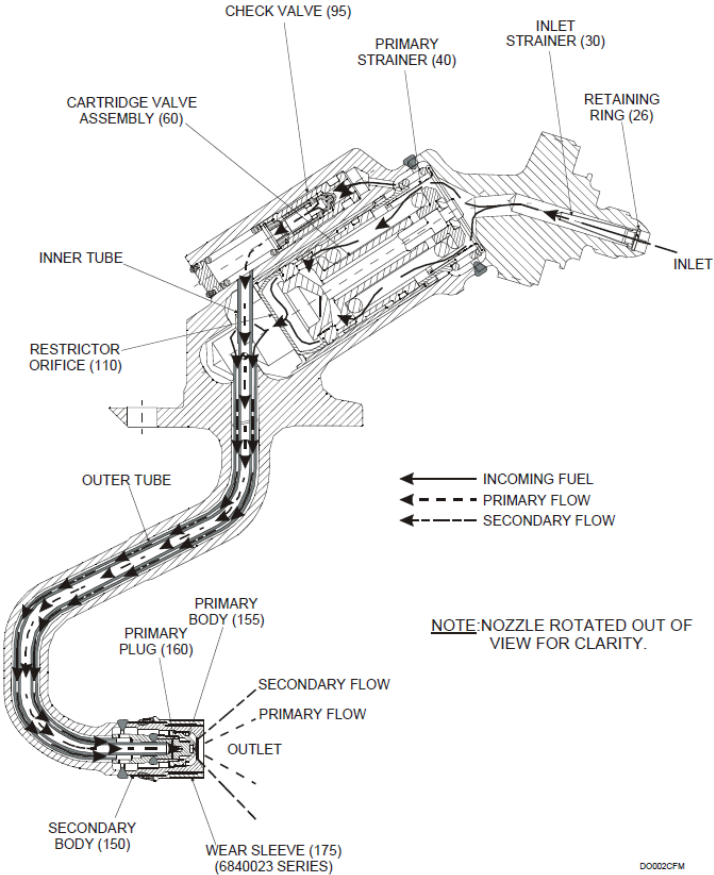


Figure 1: CFM56 Fuel Nozzle Cross-Section with Flow Paths. This cross section image was provided by Advanced Atomization Technologies.

1.1 Valve Design in Aerospace Fuel Nozzles

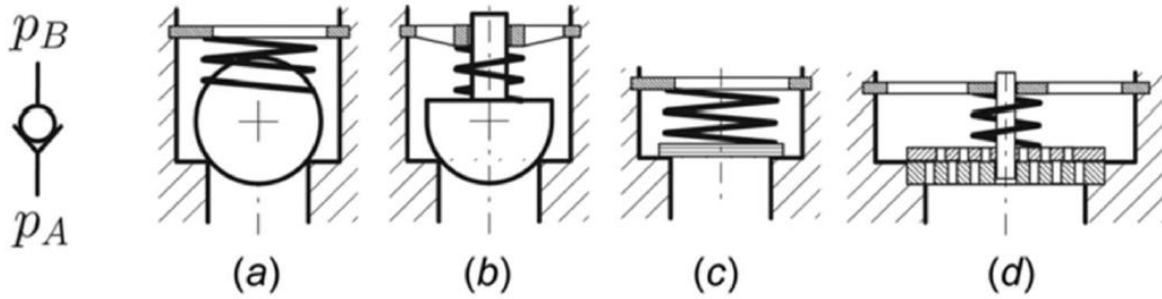


Figure 2: Check valve symbol and types: (a) ball valve, (b) poppet valve, (c) plate valve, and (d) multidisk plate valve [2]

The valves that were used in this research are based on the simple check valve design. The valves are actuated through a pressure differential caused by inlet pressure control. As seen in Fig.2 a check valve has four generalized arrangements. Both valves in the thesis research are essentially poppet valves.

Through control of the seats, stops, pressure surfaces, spring rates as shown in Fig. 3 and flow slot geometry as shown in Fig. 4, fluid flow profiles are developed to meet the needs combustion application. The flow slot in Fig. 4 is not the design of the system that was researched, but represents the unique flow openings that are used in the flow divider valve being modeled to create desired flow profiles. In the system that was analyzed in this research there are two valves that have fluid flow running in parallel. One valve is designed for low flow and actuation at the lower end of the pressure ranges experienced by the nozzle. This valve meters the primary circuit and is referred to as the check valve. The second valve is what meters the main flow profile with specialized flow geometry. This valve is referred to as the main flow divider valve and meters the secondary circuit.

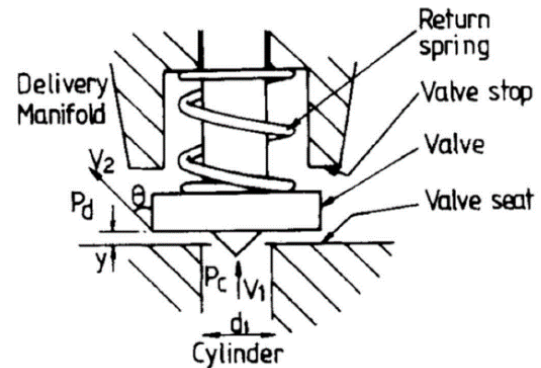


Figure 3: Simplified poppet valve diagram [2]

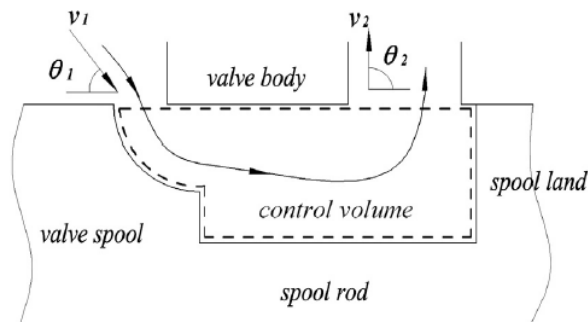


Figure 4: Example of specialized flow slot geometry used to control flow profile check valves. [6]

1.2 Challenges in Design and Manufacturing

This research is intended to be used as a design and manufacturing tool. Fuel nozzle's have tight requirements on flow profiles during testing and operation. Their responses to pressure inputs must be highly predictable, consistent, and reliable. Production of modern day fuel nozzles and valves is technically challenging and relies largely on holding consistent geometry and flow defining properties in the valve. Flow features can and are held to tolerances as tight as .0005 of an inch to create predictable flow. Of course in a manufacturing process it's not only necessary to have tight geometric and property tolerances to meet testing specifications, but the valves must be manufacturable and profitable.

Understanding and improving manufacturability of aerospace valves is a high value goal. Valves such as the ones being modeled have a daily production output of as many as 200 valves a day. Profitability of the valve can be impacted greatly from small improvements to the manufacturing yield of the program. Even though manufacturability was not a primary goal of this research, the model created could help future teams better understand causes of piece to piece variation in manufacturing.

The work done in this research can also serve as a building block to future model and data collection development. To develop more precise models and understand flow effects due to geometry variance, this model would need to be given more resolution and validation. Measurement of pressures and pressure drops at more locations throughout the fuel nozzle would have to be considered and validated. There would also have to be an effort to improve data collection methods.

2. Prior Work Review

Literature reviews for this topic cover a wide range of application with the common ground being check valve research. Focused study on fluid flow through aerospace fuel nozzles was lacking. The literature reviews for this thesis research can be broken down into five categories. Articles relating to simple valve simulations, CFD modeling of valves, valve coefficient studies, condition monitoring of check valves and vibration analysis have been reviewed.

2.1 Steady State Valve Simulation

This research was based on creating a highly accurate model of a fluid check valve system without the computational requirements of a CFD analysis. This review starts with the work done on analysis of simplified methods of check valve simulation. Simple valve analysis work is generally done with a steady state calculation. Sometimes these simplified calculations are done via iterative calculations in a computer program code. In research by H. Xie, J. Liu, H. Yang and X. Fu [1] in 2015, a hydraulic flow control check valve was evaluated through the development of steady state calculations into a MATLAB coded simulation. An image of the valve studied can be seen in Fig. 5.

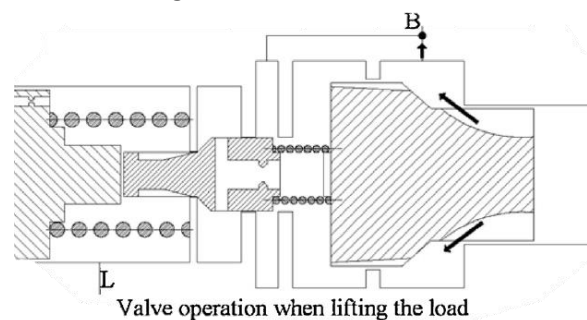


Figure 5: Cross-section of hydraulic flow control check valve studied by H. Xie, J. Liu, H. Yang and X. Fu [1]

The steady state equations were applied in MATLAB to establish a dynamic simulation. This work closely resembles the base of the intended work for this research. The basics of a calculation based valve response are also reviewed in work by A. L. Knutson [2] in 2016 LR23 for disc valves. The math involved can be applied to other check valve arrangements as well and was utilized in the work for this research. Both work by H. Xie, J. Liu, H. Yang and X. Fu [1] in 2015 and work by A. L. Knutson [2] in 2016 present significant empirical data for validation of their simplified models. Exhaustive empirical data correlation to modeling is shown to be critical in all modeling.

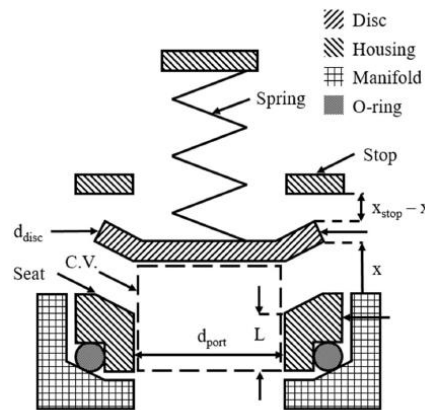


Figure 6: Cross-section of reed style check valve studied by A. L. Knutson [2]

2.2 CFD Modeling Approaches

Even though CFD modeling was not considered for this research a look into past CFD work with valves is necessary to understand model accuracy in a relativistic manner, research gaps, and some mathematical work done that relates to the research. In a study by B. K. Saha, H. Chattopadhyay, P. B. Mandal and T. Gangopadhyay [3] in 2014 a CFD analysis of a pressure regulating valve is done with a focus on understanding dynamics of the valve. A 2D model is reviewed and a function is developed to calculate forces on the spool based on actuation position. A review of work done by H. Chattopadhyay, A. Kundu, B. K. Saha and T. Gangopadhyay [4] in 2012, gives a comparison for 2D and 3D mesh formulations. Analysis of a pressure regulation valve was focused on the simulation and lacked experimental data which made the comparisons harder to validate and led to difficulty in acquiring accurate damping factors in the valve.

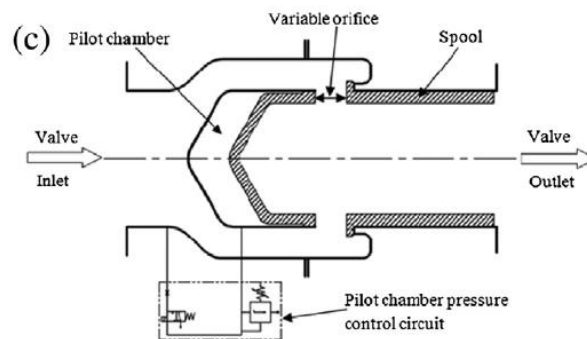


Figure 7: Cross-section of a pressure regulation valve studied by B. K. Saha, H. Chattopadhyay, P. B. Mandal and T. Gangopadhyay [3] and H. Chattopadhyay, A. Kundu, B. K. Saha and T. Gangopadhyay [4]

The work done by E. Frosina, A. Senatore, D. Buono and K. A. Stelson [5] in 2017, shows the ability and accuracy of an empirically validated CFD model. Validated CFD work was used to test new designs. New designs in the work by E. Frosina, A. Senatore, D. Buono and K. A. Stelson [5] in 2017, were also tested and validated, thus proving the methodology effectiveness.

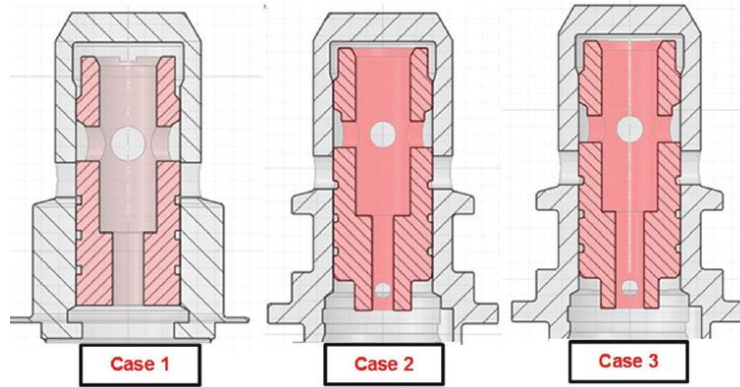


Figure 8: Cross-section of a hydraulic control valve studied by E. Frosina, A. Senatore, D. Buono and K. A. Stelson [5]

More focused work on flow slot geometries is seen in publications by Y. Ye, C.-B. Yin, X.-D. Li, W.-j. Zhou and F.-f. Yuan [6] in 2014, and E. Lisowski and G. Filo [7] in 2016. With the work by Y. Ye, C.-B. Yin, X.-D. Li, W.-j. Zhou and F.-f. Yuan [6] in 2014, complex flow groove shapes were evaluated. These flow grooves more closely represent this projects research. Y. Ye, C.-B. Yin, X.-D. Li, W.-j. Zhou and F.-f. Yuan [6] in 2014, analyzes a spool flow grooves to evaluate details such as flow area, discharge characteristics, jet flow angle, steady state flow force, and throttling stiffness. The three grooves evaluated are backed with exhaustive experimental work. E. Lisowski and G. Filo [7] in 2016 uses CFD methods to evaluate two of the same types of groove shapes as seen in the work by Y. Ye, C.-B. Yin, X.-D. Li, W.-j. Zhou and F.-f. Yuan [6] in 2014. A simulation model in MATLAB/Simulink was used with the CFD work to show the most effective throttling groove opening for a wider operating range.

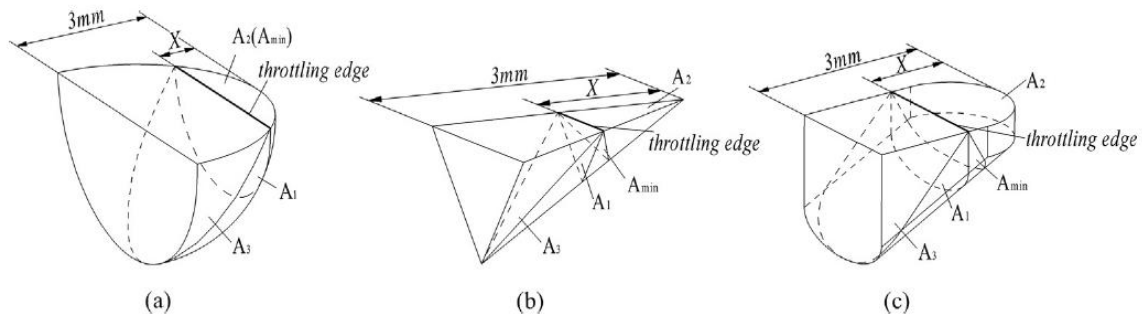


Figure 9: Geometry of the flow slots of a hydraulic control valve for construction equipment studied by Y. Ye, C.-B. Yin, X.-D. Li, W.-j. Zhou and F.-f. Yuan [6]

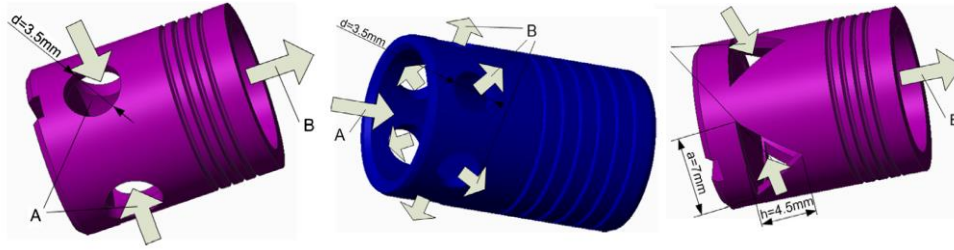


Figure 10: Images of hydraulic control valve design configurations investigated by E. Lisowski and G. Filo [7]

2.3 Valve Coefficient Studies

The generalized nature of the mathematical models that were the basis for the MATLAB/Simulink simulations in this research revealed a strong dependence on the accuracy of certain valve characteristic values. In many previous valve studies, it has been noted that damping coefficient values have been difficult to validate or accurately calculate. Understanding previous work on the valves' characteristic values allowed this research to avoid some of the pitfalls as well as generally help steer value determination efforts.

Y. Ye, C.-B. Yin, X.-D. Li, W.-j. Zhou and F.-f. Yuan [6] in 2014 shows a test setup used to verify CFD data collected on three flow groove shapes at different valve spool actuation distances. By monitoring pressure drop across the valves and flow rate discharge coefficients were pulled experimentally and compared to CFD results. E. Leati, C. Gradl and R. Scheidl [8] in 2016 primarily expands previous check valve models by considering the dynamic movement of the valve in the model. Expanding on the models leads to a thorough review of the effect of valve seat defects on the stiction force of the valve. The consideration of stiction forces result in a more realistic and closely matching comparison between simulation and empirical data.

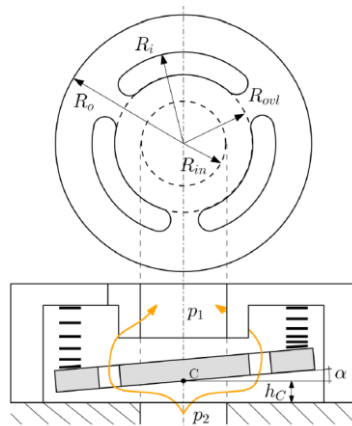


Figure 11: Image of the check valve used in the study by E. Leati, C. Gradl and R. Scheidl [8]

2.4 Condition Monitoring of Check Valves

A consideration for further research is the application of condition monitoring of check valves. In the paper by M.-R. Lee, J.-H. Lee and J.-T. Kim [9] in 2005, an advanced technique of condition monitoring for a swing style check valve is established. This particular study was done for a check valve of a nuclear power plant. The condition monitoring technique is an advanced neural network that determines check valve failure methods based on acoustic monitoring. Typical failure modes were discussed and check valve wear and foreign object blockage were evaluated experimentally. Both failure modes could be represented as leakage paths for backflow through the check valve and therefore were likely to cause acoustic emissions in the manner that this diagnostic method is likely to be able to detect. M.-R. Lee, J.-H. Lee and J.-T. Kim [9] in 2005 results showed that monitoring of acoustic emissions and application of the advanced neural network created a viable condition monitoring technique for this style valve. Failure modes such as leakage and foreign object entrapment could be considered for the future thesis research.

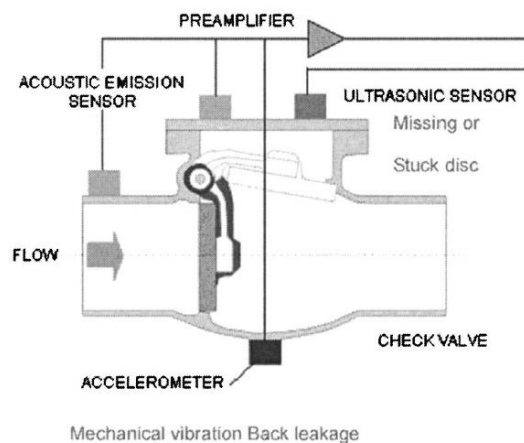


Figure 12: Cross-section of swing style check valve studied by M.-R. Lee, J.-H. Lee and J.-T. Kim [9]

2.5 Vibration Analysis of Fluid Containing Systems

Another consideration or future consideration for this research would be a more thorough look at the vibration response of the system. Although the vibration response of the valves in this system could be evaluated, it is outside the scope of this project to evaluate vibration response in the rest of the fluid filled system. There are many papers that discuss the analysis of fluid filled pipe systems or the interactions between acoustics and hydraulic systems. The method of application of the analysis would need to be computationally simple to be a viable complimentary part of the research. Many different techniques exist to evaluate the vibrations in fluid filled pipe systems.

Q. S. Li, K. Yang, L. Zhang and N. Zhang [10] in 2002, researched a liquid filled pipe system with multiple diameter sections. The pipe system is analyzed with transfer matrix methods to analyze the fluid-structure frequency responses. The sections analyzed have different materials, thicknesses and diameters. Friction coupling, Poisson coupling and junction coupling are all accounted for in the transfer matrix method described in this paper. Using a transfer function to analyze frequency response is an efficient computationally simple technique.

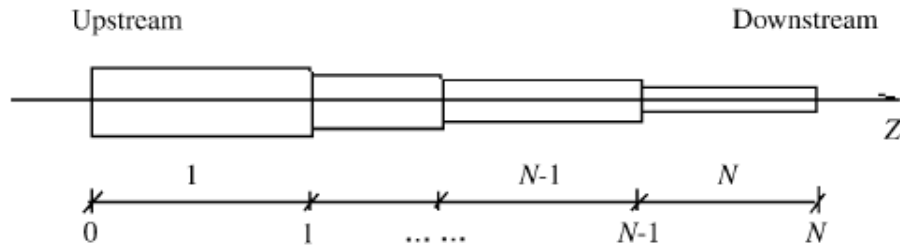


Figure 13: Diagram of the liquid filled pipe systems studied by Q. S. Li, K. Yang, L. Zhang and N. Zhang [10]

P. Persson, K. Persson and G. Sandberg [11] in 2016, did more research on reducing computational complexity for modeling fluid filled pipes and vibration responses. The work in this paper focuses on a method to reduce the computational complexity of an analysis of the vibration response in a pipe filled with a fluid. The study uses a method called interface reduction and component mode synthesis to accomplish this. Extensive work is done to prove validity of the methods. The reduced order models that were generated were compared via CPU calculation times and introduced error. Error was determined by comparing reduced order models to a full model of the coupled fluid-structure interaction analysis done with finite elements methods. The techniques used proved to reduce CPU time markedly while achieving higher accuracy than previous works using similar techniques.



Figure 14: 3D model of the pipe system studied by P. Persson, K. Persson and G. Sandberg [11]

Another paper by J. Herrmann, J. Koreck, M. Maess, L. Gaul and O. v. Estorff [12] in 2011, presents a technique for simplifying hydroacoustic fluid damping modeling. By focusing on critical factors of hydroacoustic fluid affects in a pipe system, computational requirements have been reduced. The method described accounts for frictional effects of the pipe wall and pipe cross sectional area changes. The model is analyzed in a frequency domain and the equations allow determination of resonance frequency and damping ratios of the hydraulic pipe systems. The techniques are proven through experimental techniques.

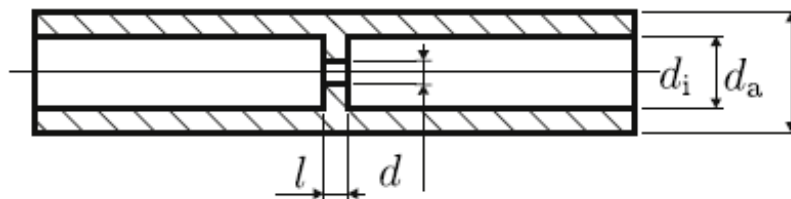


Figure 15: Cross-section the orifice and pipe studied by J. Herrmann, J. Koreck, M. Maess, L. Gaul and O. v. Estorff [12]

3. Research Gap

There is a need to develop a tool that predicts fluid flow in a fuel nozzle to a sufficiently high degree of accuracy for business design and manufacturing needs while being simple enough to operate without significant computational power. Models that exist in describing fluid flow in fuel nozzles tend to be simplified to basic steady state calculation models or complex computational fluids dynamics models. By modeling the fluid flow system dynamically using first principals, a more realistic valve system can be created. The model can be created to dynamically simulate expected fluid throughput with higher resolution and dynamic reality than is available through the basic calculation models and at a computational cost much less than CFD methods. This would allow modeling of the fuel nozzle without investment into CFD programs and computational power to run the CFD. A system model of this nature could also present opportunities for study into condition monitoring of the valves.

4. Methods

The summarized goal of this work was to create a dynamic model of a CFM56 fuel nozzle in regard to fluid flow and valve actuation. The following simulation work for the thesis research steps through the ideas that were used to build a system model that reflects reality. In order to build and validate this model the simulation model is established, flow and force calculations are defined, the experimental data collection goals and setup are established, and model optimization is reviewed.

4.1 Defining Boundaries of the Model

The model is derived from the structure of a CFM56 fuel nozzle. In this fuel nozzle the fuel flow enters in one inlet and is separated into two parallel circuits. As described previously, these circuits are metered by a check valve and flow divider valve. Fig. 16 shows a cross section of the two valves with the check valve and flow divider valve labelled.

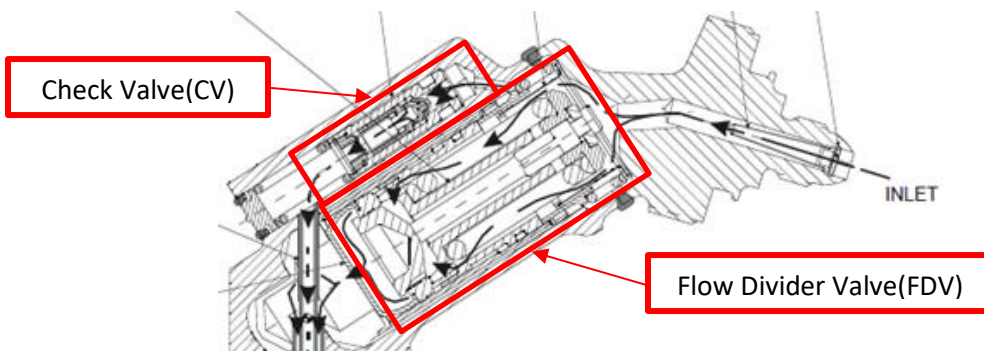


Figure 16: Cross section of CFM56 with focus on valve housing area.

For the initial model work and matching to empirical data the two circuits will be separated and each valve understood as a separate model. Each valve is basically a poppet valve with slight variance from a standard poppet valve in the flow divider valve. Fig. 17 and Fig. 18 show the control volumes for initial model work on the check valve and flow divider valve respectively. These figures are simplified drawings of each of the valves.

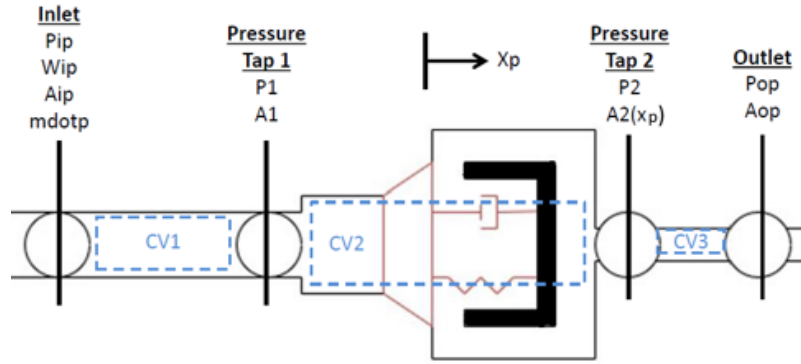


Figure 17: Simplified representation of the check valve for the primary circuit.

separated by the pressure taps. CV_1 and CV_4 represent the volume of fluid upstream of the valve systems. The outputs of that control volume will be inputs for the valve models. CV_2 and CV_5 represent the fluid flow through the valve from pressure tap to pressure tap. The areas of flow labelled $A_2(x_p)$ and $A_4(x_s)$ are dependent on the amount of actuation of the valves. By using the methods in this research, once each of the valve models shown as simplified diagrams in Fig. 17 and Fig. 18 are validated, then a combined configuration can be run to simulate the fully assembled fuel nozzle.

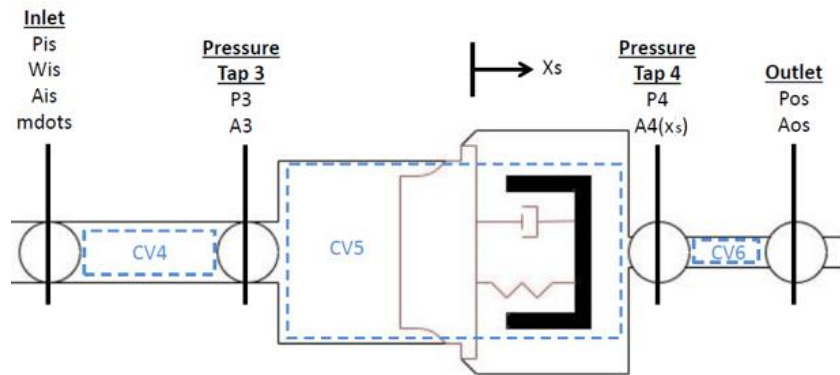


Figure 18: Simplified representation of the flow divider valve for the secondary circuit.

4.2 Forces Acting on Valves

The valves' actuation were defined by a force balance that can be broken down into several components. For the purpose of this model the forces acting on the valve will be the pressure force F_p , the spring force F_{spr} , and the seat forces F_{seat} . Other forces such as flow forces, drag forces and more have been considered in other models, but were omitted from this thesis research.

The free body diagrams in Fig. 19 shows the forces in 3 different states of actuation. In this research the forces acting on each side of the valve are assumed to be symmetrical. From left to right the diagrams represent a closed valve that has not yet actuated at all, an open valve that hasn't reached full open yet, and a fully opened valve.

The control volumes are outlined with dashed lines. The valves are shown in the diagrams as red. It's important to note the unique flow features in Fig. 18 which are a simplified representation of the flow features in the actual valve. The listed variables in each diagram represent what will be known in the validation work. Three control volumes for each circuit can be defined. They are

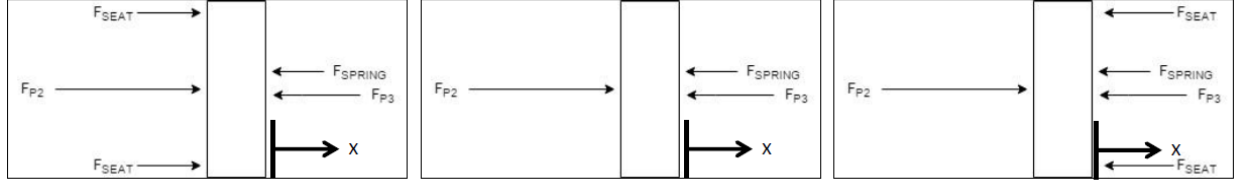


Figure 19: Free body diagrams showing 3 configurations of valve actuation. A closed valve(left), partially open valve(middle) and fully open valve(right) are shown. x represents direction of positive force and valve actuation direction

The sum of the forces affecting the valves can be written as Eq. 1. This equation is generalized in order to represent all of the possible positions of the valve.

$$F = F_p + F_{spr} + F_{seat} \quad (1)$$

Evaluating the spring force can be represented by Eq. 2. This accounts for any compression the spring experiences due to its seated constraints. Both valves being modeled in this thesis research will have significant preloads to account for.

$$F_{spr} = -k_{spr}(x + x_{preload}) \quad (2)$$

Evaluating the seat forces is another relatively simple set of equations to describe the 3 different states the seat force could be in. The valves will either be seated against the closing seat, fully open against the actuation stop seat, or somewhere in between those two.

$$F_{seat} = \begin{cases} -k_{seat}x, & \text{if } x < 0 \\ 0, & \text{if } 0 \leq x \leq x_{max} \\ -k_{stop}(x - x_{max}), & \text{if } x > x_{max} \end{cases} \quad (3)$$

Pressure force will be described as the force caused by the pressure differential upstream and downstream of the valve. It will be simplified for this preliminary work section to use an upstream area A_u and a downstream area A_d . A more detailed model is used in the actual simulation and details of how that is done are in section 4.5. The area of the check valve opening can be represented by the area of a frustum while the area of opening for the flow divider valve needs to account for a more complex opening slot and leakage flow through the balancing grooves in the valve spool.

$$F_p = P_u A_u - P_d A_d \quad (4)$$

4.3 Mass-Spring-Damper System

To simulate the valve movement realistically a mass spring damper system will be used. This 1-D parameter based evaluation method gives a non-computationally intense way to accurately simulate the valve movement while considering the interactions of all significant forces. Using the equations for a driven mass spring damper system allows us to consider the input force from the pressure differential and is shown below in Eq. 5

$$\frac{F}{M} = \ddot{x} + \frac{c}{M}\dot{x} + \frac{k}{M}x \quad (5)$$

Eq. 5 can be re-written and expressed as Eq. 6

$$\frac{F}{M} = \ddot{x} + 2\zeta\omega_o\dot{x} + \omega_o^2x \quad (6)$$

Where ω_o is the undamped natural frequency of the valve and ζ is the damping ratio. They can be calculated as shown below in Eq. 7 and Eq. 8.

$$\zeta = \frac{c}{2\sqrt{Mk}} \quad (7)$$

$$\omega_o = \sqrt{\frac{k}{M}} \quad (8)$$

The mass of the disc can be defined as seen in Eq. 9. In this mass calculation the mass of the fluid being moved is ignored as it is assumed negligible compared to the other relevant masses. This assumption was used in the reviewed literature and was also used by AATech in order to simplify their calculation and make it a viable option for industry work. This research used the same assumptions.

$$M = M_{spool} + \frac{1}{3}M_{spring} \quad (9)$$

4.4 Simulink Simulation

By re-arranging Eq. 9, which described the systems motion, to solve for acceleration we can use a series of integrators to simulate the valve in Simulink. The equation rearranged is as follows.

$$\ddot{x} = \frac{1}{M}(f(t) - c\dot{x} - kx) \quad (10)$$

A simple representation of this equation in Simulink with the force over time $f(t)$ simulated with a step input is shown in Fig. 20. The output of this system is the displacement. This is a textbook application of a mass-spring-damper in Simulink. Modifications to this idea were made to fit the simulation of the CFM56 Check Valve and Flow Divider Valve.

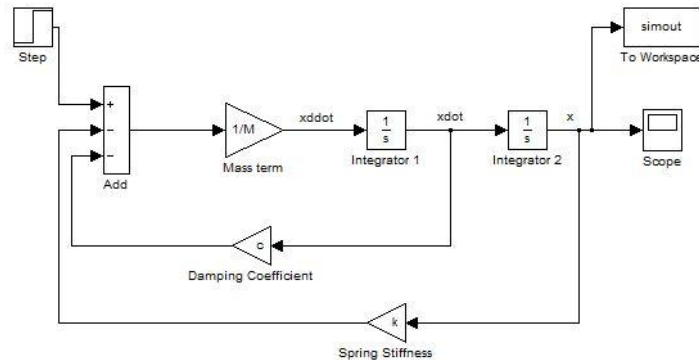


Figure 20: Simulink model of a mass spring damper system with a step input and an output of displacement. Similar to the thesis research model.

The system setup for the valves have been modeled using the mass spring damper basics as mentioned and have been augmented with code via MATLAB function blocks, and gains that represents the area in the valve that the pressure is acting on. The gains are between the input pressure and the force summation block for the system. You will also note that the Flow Divider Valve system has a “pressure_time” input which is an input of pressure data from the workspace. This allows for experimentally collected pressure data input or a custom built pressure input. The flow divider valve system setup can be seen in Fig. 21.

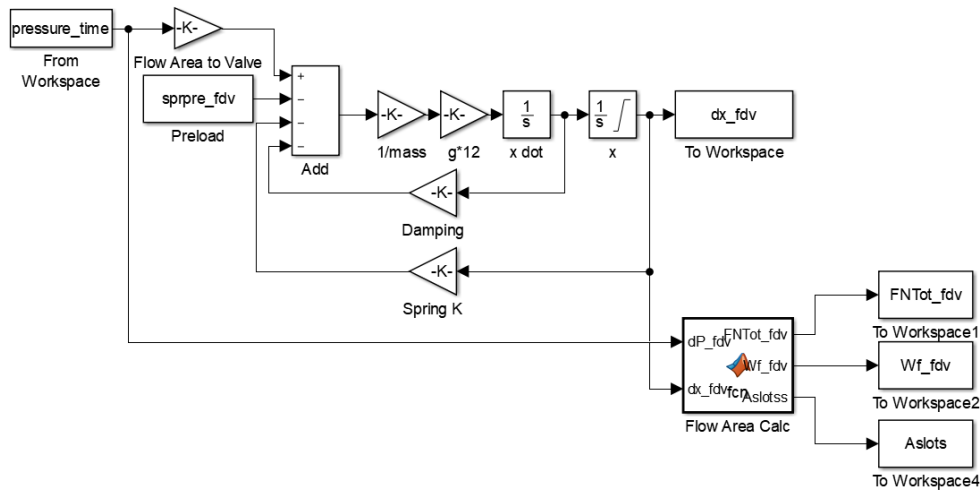


Figure 21: Simulink model of the Flow Divider Valve.

The Check Valve system can be seen in Fig. 22. In the Check Valve system the area of pressure actuation is a function block due to a change in pressure actuated area after the valve opens. This system is shown with a pressure input block that creates a pressure signal with a convenient Simulink interface.

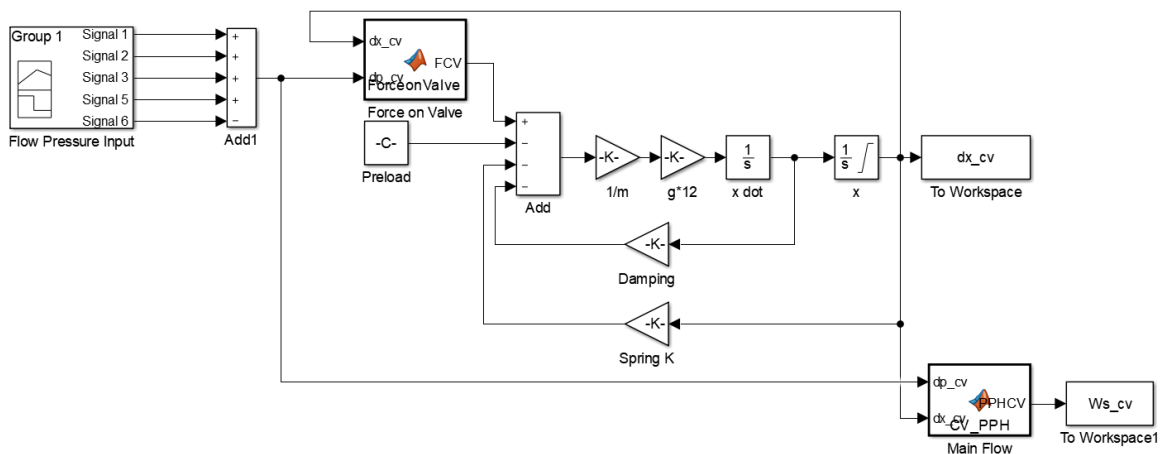


Figure 22: Simulink model of the Check Valve

This mechanism that causes an increase in area of pressure actuation is called overbalance. The mechanism is described in Fig. 23. In Fig. 23 the yellow highlight shows the area of pressure actuation and the blue lines show the fluid flow in the valve in a fully closed state(left) and then in an open state(right).

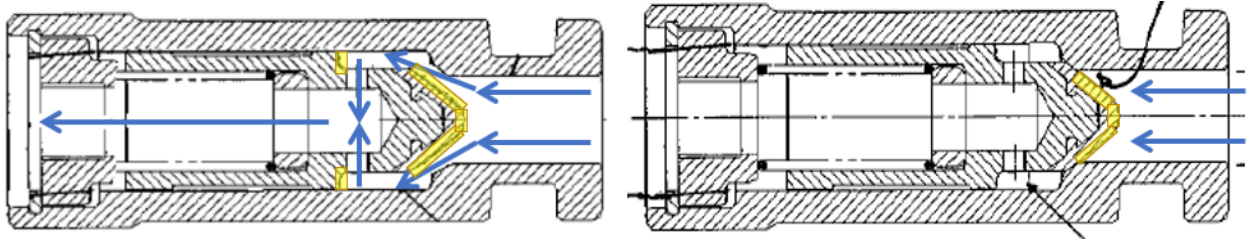


Figure 23: Comparison of area affected by pressure differential across valve in closed and open state. Highlighted yellow area indicates area of pressure affect. Blue arrows represent fluid flow. Left valve is open and right valve is closed.

The difference in Simulink setups regarding pressure input is due to the fact that using the different signal production or input methods available is important to initial testing of the simulation. Using simple clean step signal input as shown in the Check Valve was how both Simulink models were initially tested for basic operational validity. Both valves use function blocks to calculate the flow output based on valve stroke. Due to the different shapes of the valves flow areas and seats, their flow calculations are derived differently which is shown in section 4.5.

4.5 Flow Area Calculations

The valves' Simulink simulations, which are relatively basic mass-spring-damper systems, have been augmented with MATLAB function blocks to calculate the flow of calibration fluid through the specialized flow features. Due to the flow metering metering function of these valves it's appropriate to use flow number calculations to describe the flow passages. Flow number is shown as FN in the equations in this section. The derivation of the flow number calculation is based on Bernoulli's equations and assumes incompressible and inviscid flows. The flow number is a convenient way to measure the capacity of a flow system. This also lends itself to creating a system of flow number defined metering areas throughout the valves in later models to allow for the evaluation of an entire fuel nozzle.

$$FN = \frac{W_f}{\sqrt{\Delta P}} \quad (11)$$

This general form of FN equation is most often used and shows the flow rate as W_f and the pressure drop across the flow metering area as ΔP . By rearranging the equation and through substitution for equivalent flow rate equations and simplified Bernoulli's equations, the FN equation in Eq. 11 can be converted to Eq. 12 where A represents the flow area of the metering point, C_d represents the coefficient of discharge, and S is the specific gravity of the fluid.

$$FN = 19000 * A * C_d * \sqrt{S} \quad (12)$$

For all experiments in this thesis the FN can be simplified down to Eq. 13 as an aerospace calibration fluid with specification number MIL-PRF-7024 at around 80 °F is used for all tests and the specific gravity of the fluid is known.

$$FN = 16680 * A * C_d \quad (13)$$

Lastly, we need to evaluate how systems of metering areas are considered. Eq. 14-19 show the relatively simple derivations for considering systems of flow numbers. Eq. 14-16 show flow number for an entire system of metering flow points that are arranged in parallel to one another. By evaluating that

the total flow is an addition of all parallel flow points and the pressure drop is equal across all the parallel points, Eq. 16 is derived.

$$W_{fTOT} = W_{f1} + W_{f2} + W_{f3} + \dots \quad (14)$$

$$\Delta P_{TOT} = \Delta P_1 = \Delta P_2 = \Delta P_3 = \dots \quad (15)$$

$$FN_{TOT} = FN_1 + FN_2 + FN_3 + \dots \quad (16)$$

Systems with flow metering points in series can be evaluated as a series of pressure drops that equal a total pressure drop while the total flow of fluid across all points is the same as shown in Eq. 17-19. The total flow number can be derived using this concept and is shown in Eq. 19.

$$W_{fTOT} = W_{f1} = W_{f2} = W_{f3} = \dots \quad (17)$$

$$\Delta P_{TOT} = \Delta P_1 + \Delta P_2 + \Delta P_3 + \dots \quad (18)$$

$$\frac{1}{(FN_{TOT})^2} = \frac{1}{(FN_1)^2} + \frac{1}{(FN_2)^2} + \frac{1}{(FN_3)^2} + \dots \quad (19)$$

These equations were used to calculate flow in the valve simulations for both Flow Divider Valve(FDV) and Check Valve(CV). In order to accurately assess the flow over the experimental system, the models were setup so that the flow number of the fixturing being used was taken into account using the total flow number equations derived in Eq. 14-19. The flow fixtures were treated as in series flow restrictions for both FDV and CV simulation. There was also a need to account for leakage flow in the FDV, but that is covered later in this section.

The FDV is shown in Fig. 13-16 in a cross sectional view and in a 3D view with focus on the flow area. The valve is shown in all of the different flow conditions that the flow divider will experience during operations. Fig. 24 and 27 show cross sections of the valve in the fully closed state. These figures were taken from a 3D model of the FDV. Fig. 26 shows initial actuation which disengages the valve from the seat but does not engage the flow slot geometry. This flow condition is known as clearance flow. Fig. 37 shows the flow slot geometry opening further for higher flow requirements. These are the two areas of flow that are considered in the thesis research. During the simulation, the system generates a stroke distance for the valve at each data point. This valve stroke is used as an input for the valve flow functions in order to generate the simulated flow. The clearance flow and valve slot flow are considered parallel flow systems and were calculated as such.

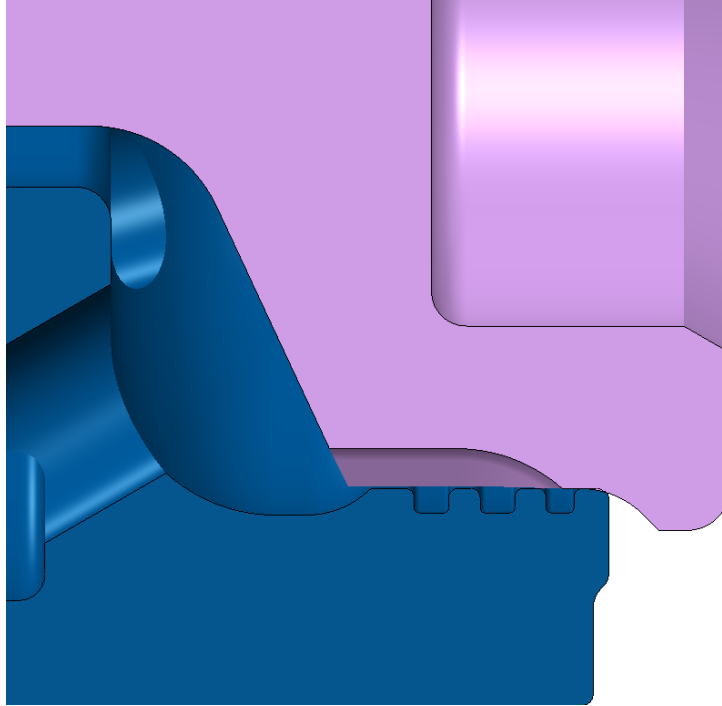
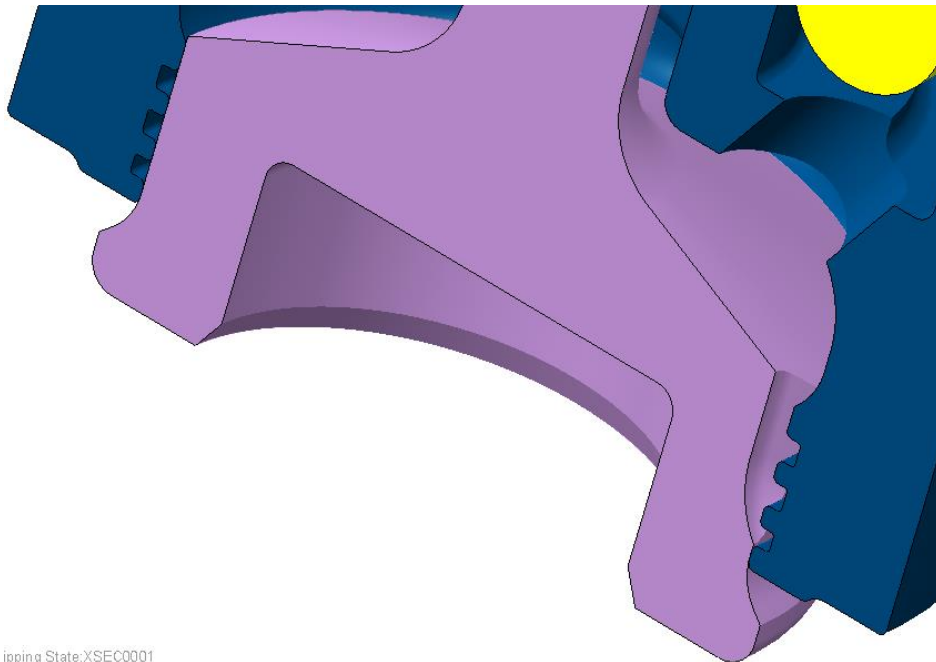


Figure 24: Cross section of flow divider valve in the fully closed position. Image taken from 3D model of the FDV.



ipping State:XSEC0001

Figure 25: Cross section of flow divider valve in the fully closed position from an isometric viewing angle to provide further perspective of the flow slot. Image taken from 3D model of the FDV.

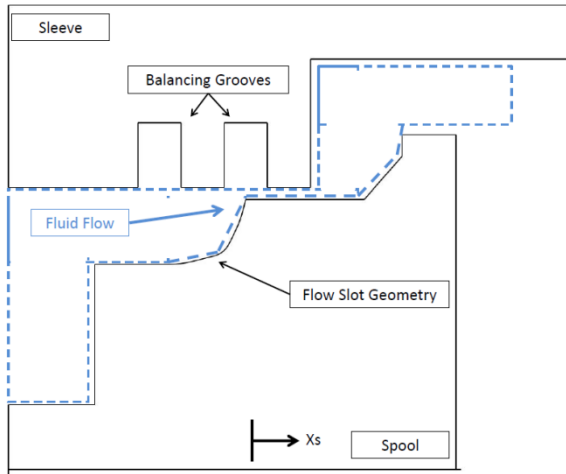


Figure 26: Cross section of flow divider valve flow area during clearance only leakage flow.

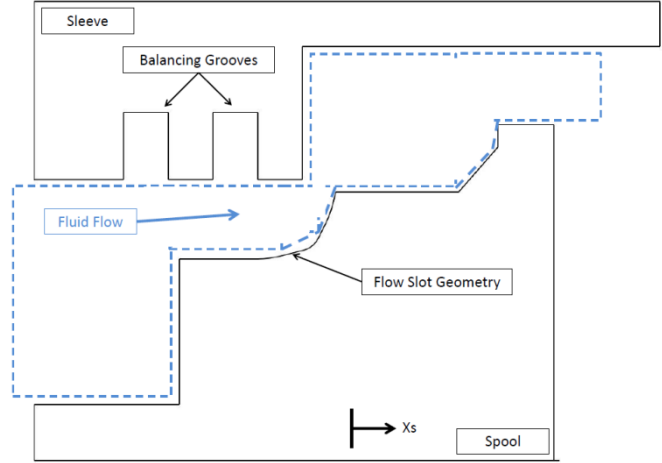


Figure 27: Cross section of flow divider valve flow area during flow slot flow opening.

The flow number calculation combines a concentric circle clearance flow number calculation combined with an AATech slot area flow number calculation. The clearance flow rate is taken as the flow between two concentric circles with an eccentricity of the shaft to the bore taken into account. The equation used is meant for applications in laminar flow in annulus where the diameter of the cylinder is much greater than the clearance radius. The equation is shown in Eq. 20.

$$W_{f_{bleed}} = \frac{\rho\pi r C_r^3 \Delta P}{6\mu L} \left[1 + \frac{3}{2} \left(\frac{e}{C_r} \right)^2 \right] \quad (20)$$

In Eq. 20 ρ represents density, r is the radius of the spool, C_r is the radial clearance of the spool, μ is the absolute viscosity, L is the bleed length, and e is the eccentricity of the shaft to the bore. Simplifying this equation for the use in this thesis means plugging in the fluid properties of MIL-PRF-7024 at around 80 °F, converting units to fit our flow rate of lbs/hour, and converting the eccentricity factor into a single variable. This simplification leaves the equation as seen in Eq. 21.

$$W_{f_{bleed}} \approx 399958855.8 \frac{r C_r^3 \Delta P e_{bleed}}{L} \quad (21)$$

The slot area flow number calculation for the flow divider valve is taken from a tool used by Advanced Atomization Technologies. The function generates the area perpendicular to the flow through the slots through a combination of ellipsoids, triangles, and other geometries relevant to the specific FDV flow slot geometry which can be seen in Fig. 24 and 25. This tool is proprietary, and the exact calculation is omitted from this report due to this. However, the curve of the flow area being calculated is shown in Fig. 28. In Fig. 28 the curve was generated by using Advanced Atomization Technologies area calculator with a nominally dimensioned valve and a linear valve stroke increase. The curve follows expectation and has been tested by Advanced Atomization Technologies for accuracy to real hardware. Time was used as the x-axis for the figure to maintain intellectual property security.

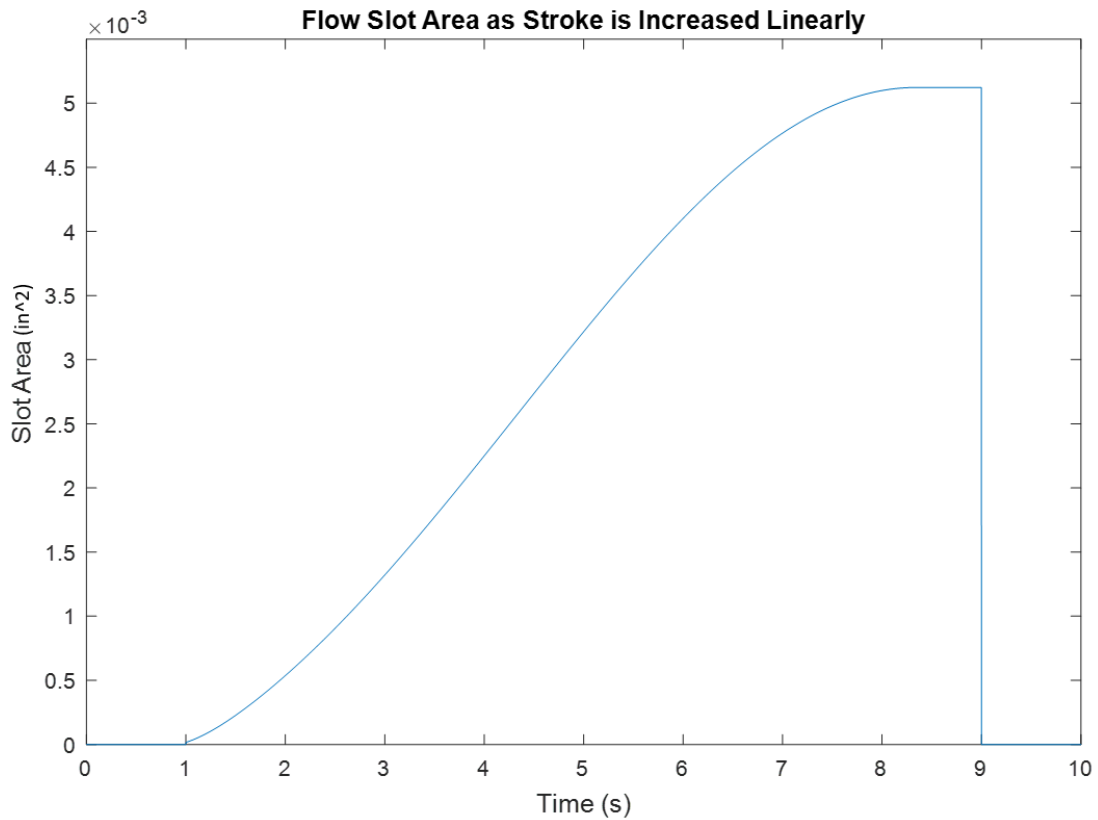


Figure 28: Cross section of flow divider valve flow area during clearance only leakage flow.

This flow slot area calculator requires the input of specific dimensional data that is relevant to Advanced Atomization Technologies valve production and design. Several slot dimensions are considered in the calculation. This method of slot area evaluation allows the calculator to be used more effectively for manufacturing variation evaluation and design of experiments work.

The check valve that controls primary fuel flow in the fuel nozzle uses the same core modeling techniques as described for the FDV in that a flow number is generated using the stroke and the flow area. An accurate cross section of the valve in a closed and open state can be seen in Section 4.4 in Fig. 12. A simplified cross section of the flow area and an explanation of the flow area from a dimensional standpoint can be seen in Fig. 29 and 30. There is no leakage flow or flow slot geometry. The area between the valve seat and the poppet can be described by calculating the frustum of a cone. Eq. 22-25 describe this area with regards to Fig. 30.

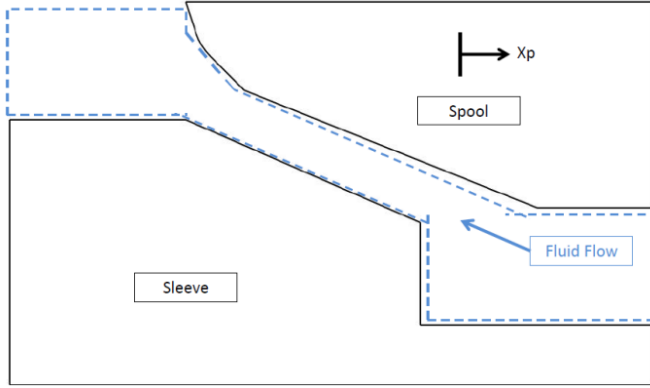


Figure 29: Cross section of check valve flow area.

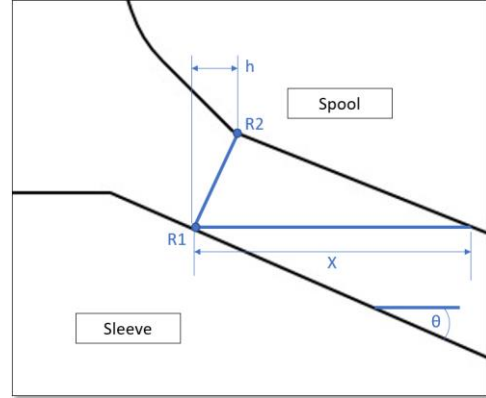


Figure 30: References for area between valve seat and poppet.

$$A_{cv} = \pi(R_1 + R_2)\sqrt{(R_1 + R_2)^2 + h^2} \quad (22)$$

$$R_2 = R_1 - ((X \sin \theta) \cos \theta) \quad (23)$$

$$h = (X \sin \theta) \sin \theta \quad (24)$$

$$A_{cv} = \pi(R_1 + (R_1 - ((x \sin \theta) \cos \theta)))\sqrt{R_1 - (R_1 - ((x \sin \theta) \cos \theta)) + (x \sin \theta) \sin \theta} \quad (25)$$

4.6 Experimental System Setup

The experimental setup for this thesis was established to allow for validation of the valve stroke and valve flow simulations. Due to the resource availability, the systems for stroke validation and the system for flow validation had to be separated. Both systems ran in parallel during the testing.

All model validation and data collection were done at AATech facilities and using AATech equipment and software. The testing was done on AATech's newest test stands with the highest accuracy. The accuracy of these test stands, and their sensors are described later in this section. The test stands are also used for AATech production hardware. The production tests stands' data collection capability was augmented with a compliment of supplemental sensors that affix directly to the fixturing that contained the valves. The production test stands allowed for flow rate and pressure drop to be collected in one data set while the fixture sensor package allowed for valve stroke and pressure drop data to be collected in another data set. All testing was done using an aerospace calibration fluid with specification callout of MIL-PRF-7024 type II at 80 °F ±5 °F.

Production test stands were purpose-designed and built to meet needs of AATech’s production lines. The specific test stands used for this research have a data acquisition rate of up to 1 kHz. The system used GE Unik Pressure Transducers to obtain upstream pressure. The flow of the calibration fluid was measured with different sensors depending on the flow rate. If flow was between 0-225 pounds per hour (PPH) then the flow was measured with a Micromotion CMF 010. If the flow was between 225-1000 PPH then the flow was measured with a Micromotion CMF 025. The test stand outputs data to a .csv file which can be pulled into the MATLAB simulation. One note about the flow data that needs to be considered is that the test stand has a built-in damping algorithm to keep anomalous data from the sensor from reaching the output file. The stand uses a “damp rate” of 0.8sec to review data and collect averages of small portions of data to smooth responses. Any anomalous or outlier flow readings that occur within a 0.8sec timeframe are averaged against the other data points in that 0.8sec time set to smooth the output data.

Since the production test stands do not have a need to track valve stroke, the setup for this research used a specialized fixture with its own set of sensors and data collection unit. A PHILTEC Model RC171 displacement optical sensor was used to collect data on valve spool movement. This instrument has a data collection capability of 20kHz and has a resolution of 0.56 mv/μm. The sensor is suited for the calibration fluid used in testing. In order to use the optical stroke measurements with the established valve simulation, the experimental fixture needed to also record high resolution pressure data that was in time step with the stroke movement. The Kulite EXTEL-190 transducer was used to evaluate pressures and pressure dynamics. The sensors collected pressure information upstream and downstream of the valve. The EXTEL-190 is an analog sensor and is therefore only limited by the data collection rate of the system it’s connected to. The sensor can handle up to 3000PSI which far exceeds pressure ranges that the valve systems would be tested in. Overall, the system can collect data at a rate of 20kHz.

All data from the sensor package attached directly to the fixturing was collected with a Dewesoft Sirius data acquisition device. The Dewesoft is a flexible and user friendly data acquisition device that AATech already had access to. This device readily accepted the sensors being used in testing. The Dewesoft has a 1MHz sampling rate capability per channel so it fit the needs of the sensors in the research.

Valve Testing Equipment			
Purpose for Experiment	Make	Model	Pertinent Notes
Data Acquisition	Dewesoft	Sirius i	Sample Rate: 1MHz Analog and Digital Inputs
Pressure Sensor	Kulite	Extel-190 M series	Sample Rate: Infinitesimal Pressure Limit: 3000 PSI Operating Temp: -65 to 525 °F
Displacement Sensor	Philtec	RC171	Sample Rate: 20kHz Linear Range: 4.7-8.4mm Sensitivity: 0.56mv/μm Pressure Limit: ~500 PSI Operating Temp: -55 to 175 °F

Table 1: Equipment table for valve testing

System setup during experimentation involved two separate data collection sets as mentioned earlier in this thesis. Data collection was done through the output of files with delineated test data by both the Dewesoft and the test stand DAQ. The Dewesoft system involved the two Kulite pressure sensors, the Philtec optical sensor, a DC power supply, and a laptop for the Dewesoft software. The DC power supply was needed to power the optical sensor which runs on a voltage of between 12VDC and 24VDC. The voltage supplied was 18VDC for the experiment. The test stand system was a stand alone system that required no setup. The systems were only connected via the common fluid flow channels shared. Both systems output .csv files. These files were converted to .xlsx files for easy MATLAB manipulation during simulation work. A simplified representation of the systems are shown in Fig. 31.

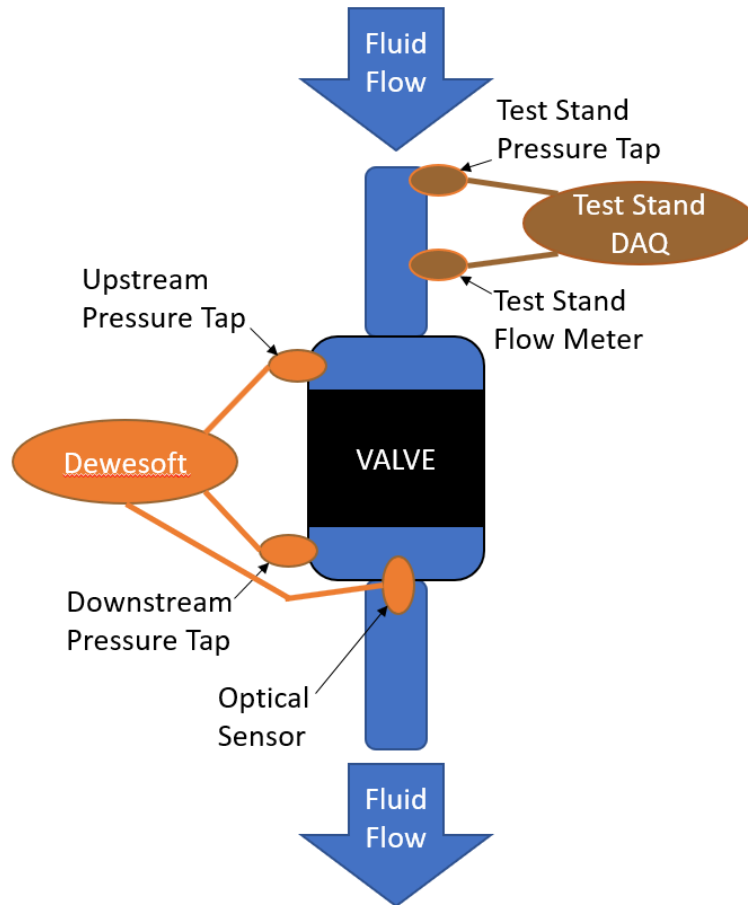


Figure 31: Simplified diagram of the experimental system used for data acquisition.

Specialized test fixturing was designed and built for the experimental work. The fixturing to house valves and test sensors during testing was made from acrylic. The material was selected because the index of refraction matched the calibration fluid and the strength properties were sufficient to handle the pressures that testing was expected to reach. The matching index of refraction offers unaltered viewing of the system during operation. This opens up the testing to possible interaction of vision systems. Although the scope of this research doesn't encompass vision systems, AATech may want to employ them in future work. The clear material was also convenient for proper placement of sensors in the fixturing. The fixturing has features to allow attachment of the microphones for pressure sensing upstream and downstream of the valve. The fixturing also has a fitting to accept and lock in an optical fiber for the optical sensor data collection.

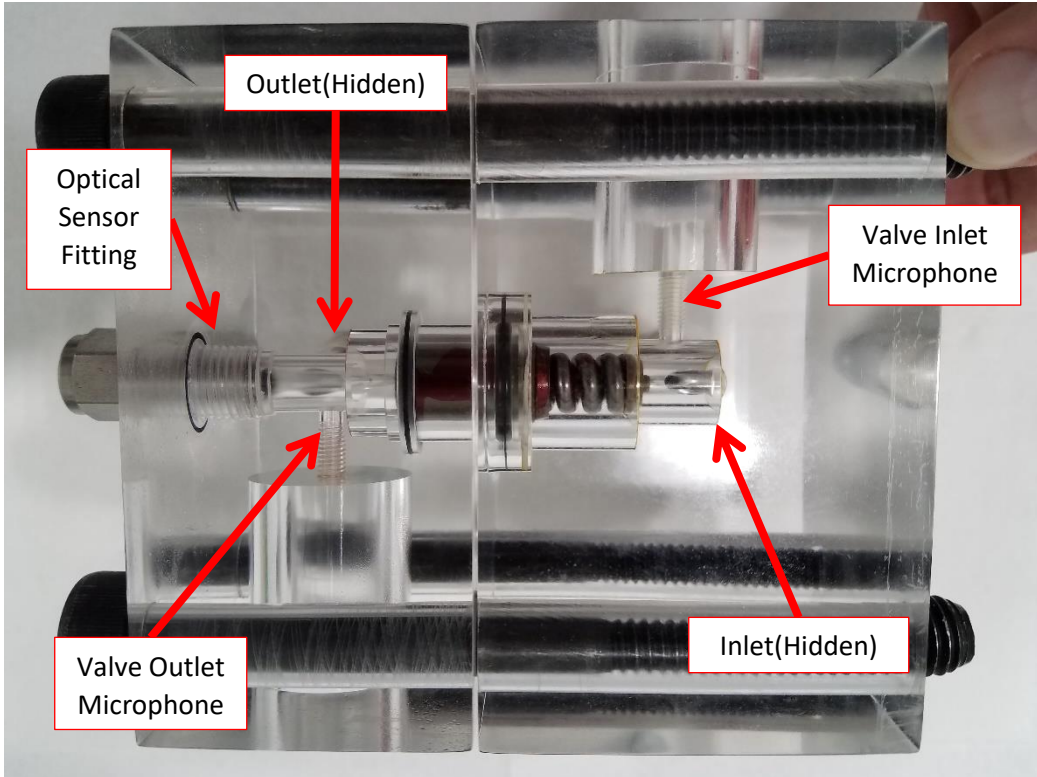


Figure 32: FDV fixturing for fluid pressure and laser displacement measurement and data collection. Made out of acrylic.

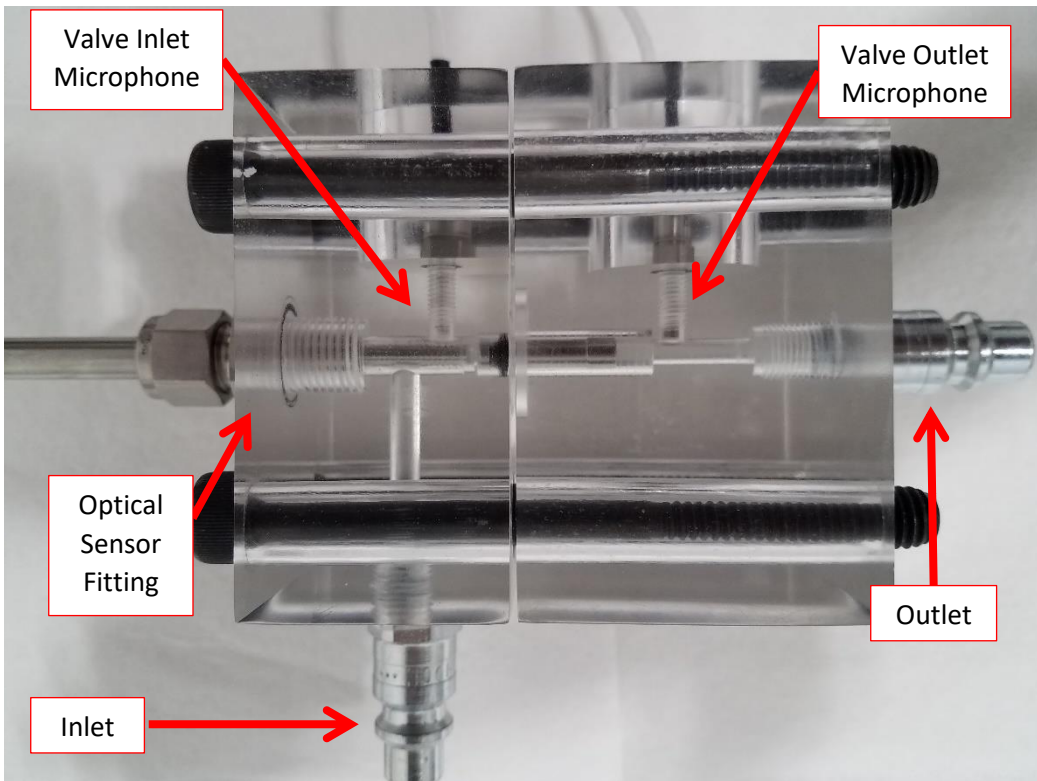


Figure 33: CV fixturing for fluid pressure and laser displacement measurement and data collection. Made out of acrylic.

Fig. 32 and 33 are images of the fixturing designed and built for the testing of the FDV and CV respectively. The pressure tap holes for the microphones as well as the optical sensor fitting. The inlets and outlets are also labelled in the images and consist of Hanson fittings to facilitate connection to AATech fluid flow test stands. The fixturing was designed with the intent of matching the upstream and downstream flow passages to the flow numbers of production valve flow testing hardware for the purpose of consistency.

In addition to the special fixturing and data acquisition setup the test valves themselves had to be modified. Mirror surfaces had to be created or affixed on both valves to allow the optical sensor to accurately determine positional data. For the FDV, the optical sensor is downstream of the FDV. In the CV fixturing the optical sensor fitting is upstream of the valve. On the FDV, the location where a mirror could be affixed without affecting flow and valve behavior was on the downstream side of the valve spool. A glue was used to affix a lightweight mirror to the valve spool. It should be noted that even though the mirror was light weight, the test valves were weighed to determine mass properties after the mirrors were glued on to ensure accurate simulation. The CV had to be modified slightly to create a mirror surface for the optical sensor to reflect. The tip of the CV was polished to create a mirror surface. This surface faces upstream. Fig. 34 and 35 show the mirror on the CV. Fig 36 and 37 show the mirror on the FDV.



Figure 34: Mirror surface in the assembled CV.



Figure 35: Mirror surface on poppet out of assembly.



Figure 36: FDV with mirror glued to spool in assembly.



Figure 37: Mirror glued to spool out of assembly.

In the experimental setup for this research certain pre-test experimental work had to be done for each fixture as well. Each fixture had to be flow tested to evaluate the flow number for that fixture. This was done by testing each fixture at different pressure points across a wide pressure range and taking an average flow number from the calculations at each flow point. Results of the FN checks can be found in Section 5.1. The optical sensor had to be configured for each fixture setup as well. This had to be done to establish the calculation for converting the voltage output of the sensor into displacement of the mirrored surface of the valves. To do this the optical sensor was locked into a distance that would make the valves' strokes fall completely within the sensor's linear range. The valves were moved incrementally through the optical sensors linear range and a voltage reading at each increment was recorded. A table of the configuration work was created and a best fit equation was determined and used for the test data of each valve. Results of the configuration can be found in Section 5.1.

Geometric data collection was also critical to this research and was collected using AATech gage lab. All necessary equipment is kept calibrated and available to accomplish the goals of this thesis research. All slot dimensions, valve mass properties, and spring rates were accounted for and measured using AATech facilities.

4.7 Experimental Data Collection Plan

In order to effectively hone the simulations that have been created for this research, the experimental data has to be sure to cover a couple different operational situations and valve actuation plans. This is important to showing the simulation's ability to effectively match varying cases of flow profile possibilities. The profiles were developed with a couple main ideas in mind.

The decided upon profiles for both the FDV and CV need to cover the valves' full operational range, they need to cover typical production testing, and they need to cover situations that typical testing wouldn't run into. With these ideas the three testing profiles for each valve were produced. The first testing profile steps through a wide pressure range in small enough increments to give the profile fidelity across those ranges. This test profile was done with the normal pressure impulse as the production test stand pressure checks. This pressure impulse dictates how quickly the test stand ramps the pressure up to the next designated pressure point. The second profile is the production test for this fuel nozzle valve. This profile tests a range of pressure points that were deemed critical to the operation of this valve from an operational standpoint when the valve was originally designed. The pressure impulse for this was left at production levels. The third profile created was intended to create a situation where the valve system experiences forces and pressure fluctuations that are outside normal production testing standards. This test uses the highest pressure impulse producible by the test stands available. The thoughts behind this were to hopefully create a noticeable overshoot of the valve spool in order to identify the valves damping after overshoot. All pressure profiles for the FDV and CV can be seen in Table 2 and Table 3 respectively. All three test profiles include an air bleed and an initial valve cycling part. These two portions of each test ensure that the valve is encompassed by liquid, is settled in the fixturing properly, and is clear of debris. Due to the frequent disassembly and reassembly during testing the startup sequence for each profile is critical to replication of test conditions.

Test Profiles for FDV		
Test Plan Description	Summary of Test Steps	Test Setup Notes
Continuous Step Increase	<ol style="list-style-type: none"> 1. Bleed out air(low press. start) 2. Run Circuit up to 250 PSI and back down to 50 PSI 3. Run Circuit up to 250 PSI and back down to 50 PSI 4. Step from 25-250PSI with 25PSI steps. 	<ul style="list-style-type: none"> • Uses production pressure impulse. • Highest fidelity continuous test.
Normal Production Testing Cycle	<ol style="list-style-type: none"> 1. Bleed out air(low press. start) 2. Run Circuit up to 250 PSI and back down to 50 PSI 3. Run Circuit up to 250 PSI and back down to 50 PSI 4. 60 PSI 5. 70 PSI 6. 166.57 PSI 7. 227.61 PSI 8. 166.57 PSI (hysteresis) 	<ul style="list-style-type: none"> • Uses production pressure impulse. • Closely resembles production test procedure for valve.
High Impulse Testing	<ol style="list-style-type: none"> 1. Bleed out air(low press. start) 2. Run Circuit up to 250 PSI and back down to 50 PSI 3. Run Circuit up to 250 PSI and back down to 50 PSI 4. 2X at 0 PSI – 60PSI – 0PSI 5. 2X at 0 PSI – 70PSI – 0PSI 6. 2X at 0 PSI – 100PSI – 0PSI 7. 2X at 0 PSI – 167PSI – 0PSI 8. 2X at 0 PSI – 227PSI – 0PSI 	<ul style="list-style-type: none"> • Uses fast pressure impulse • Impulse rate causes slight overshoot of pressure point

Table 2: Test profiles for Flow Divider Valve experimental work

Test Profiles for CV		
Test Plan Description	Summary of Test Steps	Test Setup Notes
Continuous Step Increase	<ol style="list-style-type: none"> 1. Bleed out air(low press. start) 2. Run Circuit up to 80 PSI and back down to 5 PSI 3. Run Circuit up to 80 PSI and back down to 5 PSI 4. Step from 10-70 with 10PSI steps. 	<ul style="list-style-type: none"> • Uses production pressure impulse. • Highest fidelity continuous test.
Normal Production Testing Cycle	<ol style="list-style-type: none"> 1. Bleed out air(low press. start) 2. Run Circuit up to 80 PSI and back down to 5 PSI 3. Run Circuit up to 80 PSI and back down to 5 PSI 4. 35 PSI 5. 70 PSI 	<ul style="list-style-type: none"> • Uses production pressure impulse. • Closely resembles production test procedure for valve.
High Impulse Testing	<ol style="list-style-type: none"> 1. Bleed out air(low press. start) 2. Run Circuit up to 80 PSI and back down to 5 PSI 3. Run Circuit up to 80 PSI and back down to 5 PSI 4. 2X at 0 PSI – 35PSI – 0PSI 5. 2X at 0 PSI – 70PSI – 0PSI 	<ul style="list-style-type: none"> • Uses fast pressure impulse • Impulse rate causes slight overshoot of pressure point

Table 3: Test profiles for Check Valve experimental work

4.8 Model Optimization Technique

Due to the nature of the models for this research, the optimization had to be done in two parts. The first part of the optimization was done on the valve stroke length simulation via the mass spring damper system. The second part that was optimized was the flow calculation based on the flow area function. This flow function in Simulink uses the stroke length from the mass spring damper system to calculate flow area and expected flow output. Without a well optimized valve stroke simulation, the flow area calculation will not be able to match reality.

The optimization work was done using a MATLAB program function “fminsearch” paired with a root mean square comparison. In order to do this, the root mean square value of the difference between the measured and simulated data was generated first. The output for the experimental data would be stroke measurement or flow measurement, depending on which part of the simulation is being optimized.

First, the difference between the output vectors of data are taken. A MATLAB function “rms” is used to calculate the root mean squared value of the difference vector. Equation 26 shows an example of this with the stroke data being evaluated with “rms”.

$$RMS_{Stroke} = 'rms'(Stroke_{sim} - Stroke_{measured}) \quad (26)$$

In Eq. 26 RMS_{Stroke} indicates the root mean squared value of the difference vector, $Stroke_{sim}$ indicates the output vector of the valve stroke simulation, and $Stroke_{measured}$ indicates the vector of

stroke measured using the optical sensor. This same arrangement of equation was used for flow optimization with the simulated stroke and measured stroke vectors being replaced with simulated flow and measured flow respectively. After calculating the root mean square value of the difference vector the MATLAB function “fminsearch” was used to bring the simulation to as close a match as possible by varying certain parameters in the simulation.

The MATLAB function “fminsearch” is a nonlinear programming solver, that searches for the minimum value of a multivariable function. It allows the selection of the variables to be modified in order to achieve the minimum value of the function. By reducing the value of the root mean square value of the difference vector, the “fminsearch” function iteratively brings the simulation output closer to the measured output and thereby optimizing the simulation relative to reality.

Each of the two optimizations rely on different sets of variables. For this research the optimization of the stroke length was done with the spring preload, damping coefficient, and pressure actuation area. All other features were defined from empirical work or were not included in calculations. The optimization of the flow calculation considers the eccentricity, orifice discharge coefficient of the flow slots and orifice coefficient for the bleed. All other variables in the flow calculation are based on empirical work or were not included in the calculations.

5. Results

5.1 Experimental and Empirical Data Collection

Empirical and experimental data collection was a several stage effort. Empirical data was collected on the valves to accurately build the simulations, the fixtures to build their flow effects into the simulations, and the equipment calibration to ensure accuracy of equipment reading. All empirical data collection was done at AATech with AATech equipment.

The measurements of the valves were excluded from this report to keep confidentiality of design and are not necessary to relay the effectiveness of the techniques tested in this thesis. The flow fixtures were evaluated at several points of flow without any valves in them to determine their own flow numbers and the effect that would have on simulation. Calibration of the optical sensor was accomplished with drop gage readings at specific distances from the end of the optical sensor. Half of the fixture that houses the optical sensor was placed in a way where the optical sensor and mirrored surface of the valve could be submerged in calibration fluid, while the other half of the valve could be dry and affixed to a drop gage. The drop gage was then adjusted to specific distances over the linear range of the sensor.

The FDV fixturing was run at the pressure points shown in Table 4. The average FN was calculated as 98.98 and used for the FDV flow simulation.

FN for FDV Fixture			
Pressure Input Setting (PSI)	Pressure Reading (PSI)	Flow (PPH)	FN
10	9.873	323.3	102.8919
20	20.29	450.1	99.92358
30	30.52	540.9	97.90947
40	40.74	632.9	99.15728
50	49.95	698.7	98.86054
75	75.26	852	98.2104
100	99.54	981.5	98.37653
150	150.3	1183	96.4951

Table 4: FDV FN testing and calculations used for simulation development.

Sensor calibration data was collected in the manner mentioned previously in this report and the data was plotted as seen in Fig. 38. The drop gage readings as compared with the voltage readings from the Dewesoft software were used to generate a linear equation of best fit. The coefficient of determination of the line is shown in Fig. 38 as .9744. The line is a good fit to the data. The linear equation shown was used to convert the Dewesoft voltage data from all FDV tests into valve displacement.

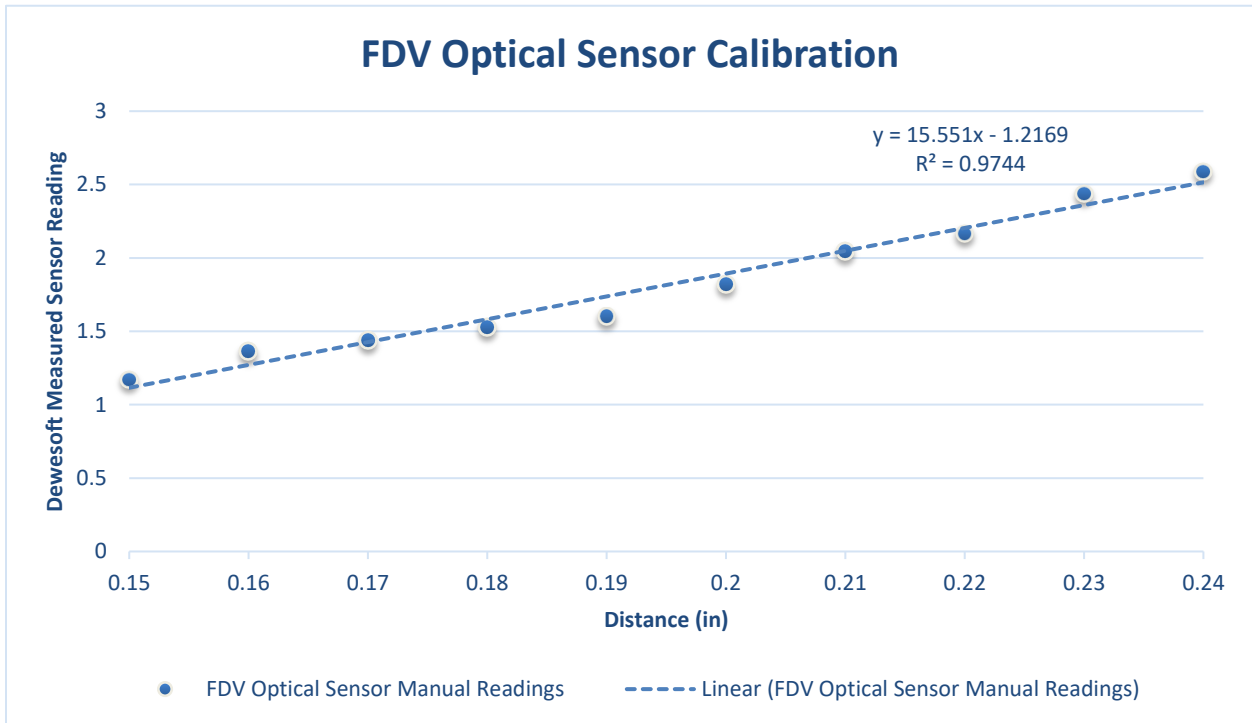


Figure 38: Data plot of optical sensor calibration with linear best fit line

After completion of all valve, fixture, and sensor empirical work all five FDV's were run through their established test programs as described in Table 2 in Section 4.7 of this report. During the data collection an issue showed in the optical sensor measurements. The sensor presented stroke data that seemed to indicate some sort of violent high frequency resonance with the valves. Further investigation revealed that although some of the reported high frequency valve movement matched with the pressure fluctuations seen from the pressure sensors during testing, the more extreme examples and some other variations in the flow did not match pressure fluctuations or valve movement expectations. Investigation during testing showed that the main contributor to optical sensor failure and flawed data collection was cavitation or bubble formation just downstream of the flow slots in the FDV. Fig. 39 and Fig. 40 show examples of the FDV during testing at flow points where the valve is open, and the flow slots are engaged in the flow. The first figure shows an example of normal operation with relatively accurate data collection and the second figure shows an example of the cavitation effect that caused flawed data collection during tests. It should be noted that the flawed sensor recordings were not only recorded during active flow states with cavitation. Some instances of bubbles becoming lodged in locations that affect the optical sensor line of sight were recorded and show up in the experimental data. More examples and discussion of how this cavitation affected the research can be found in Section 5.5.



Figure 39: FDV during data collection. Shows test pressure point with no cavitation/bubble formation.



Figure 40: FDV during data collection. Shows test pressure point with cavitation/bubble formation.

Due to the cavitation and bubble formation the Dewesoft data had to be post processed before being applied and used in simulation work. Acceptability of the data was evaluated based of valve stroke reading stability. Since the expectation was that the valve would not move much during the pressure set points it could be deduced that data at pressure set points that displayed behavior indicating rapid extreme movement were due to the failure of the optical sensor due to bubble interference. Sudden repeating changes of greater than .001" of valve movement was used as a gage for this evaluation. This expectation was used to evaluate the data for sections of experimental code that were most likely affected by the cavitation and bubble formation. Data that experienced fluctuations as described previously were then manually adjusted by means of removing grossly inaccurate pressure set points in order to provide cleaner simulation input, output, and comparison. The cavitation was most severe between inlet pressures of ~90PSI-225PSI. An example of the unprocessed Dewesoft data can be found in Fig. 106 in Section 5.5. This cavitation and evaluation of data left only two sets of testing profiles as viable options for simulation work.

The High Impulse Test program and the Continuous Step Increase program had the largest amounts of useable data. Fig. 41 and Fig. 42 show the data from all 5 of the valves from the High Impulse Test program and the Continuous Step Increase program respectively after manual adjustments were completed. The Dewesoft setup collected valve stroke and pressure drop. The valve stroke during testing is what's reported in Fig. 41 and Fig. 42. These figures depict a comparison of how each valve performed relatively to the other valves during the testing regarding stroke.

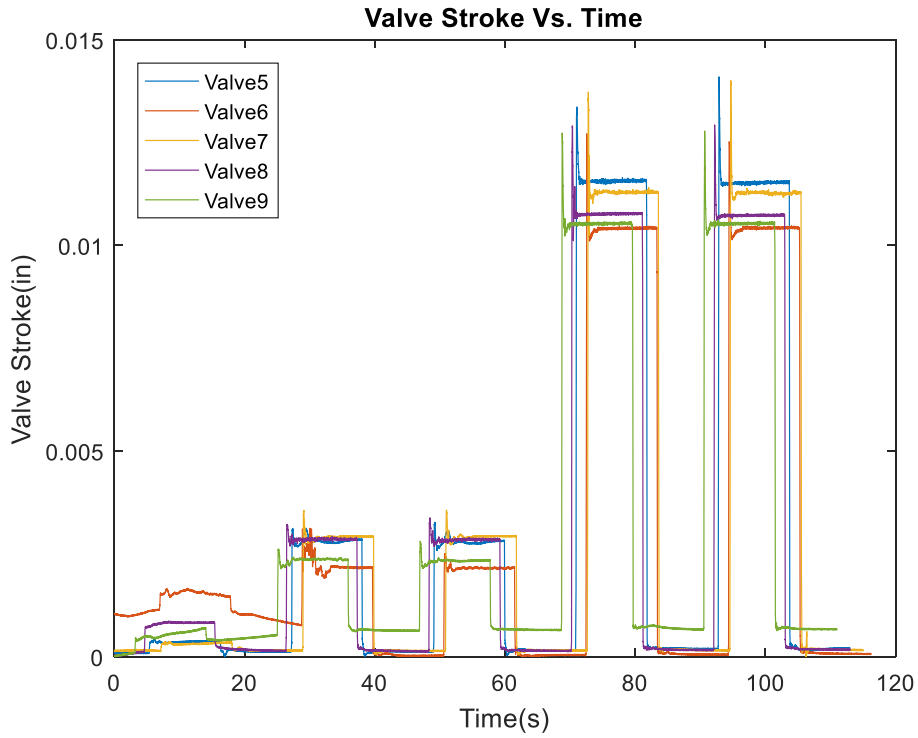


Figure 41: All FDV's stroke data collected from the High Impulse Testing program

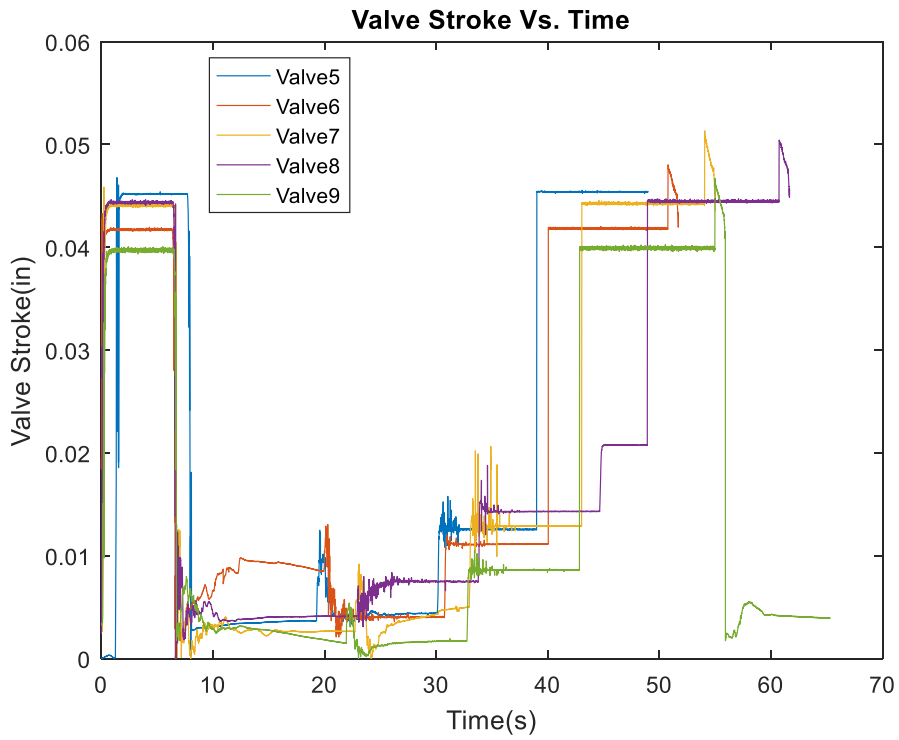


Figure 42: All FDV's stroke data collected from the Continuous Step Increase program.

Although Fig. 41 and Fig. 42 were processed to remove most gross inaccuracies in the sensor data, it was impossible to eliminate all and still maintain value for this research. Most sudden changes in valve displacement seen in the data was a result of cavitation interference. Focusing on the plots between time stamps 10 and 30 seconds reveals other optical sensor inconsistencies. The timing of the tests does not align well because of the post processing which did not allow for a convenient start point for all data sets. The figures are a good comparison for the differences in valve stroke as measured empirically.

Test stand data was also collected for all 5 valves. There were no issues with the test stand data collection. The test stand data that correlated to the useable Dewesoft data was used for simulation experimentation. Fig. 43 and Fig. 44 show the results of each of the valves for the High Impulse Testing program and the Continuous Step Increase program respectively. The test stand collected flow and pressure data and the flow data is reported in Fig. 43 and 44. These figures depict a comparison of how each valve performed relative to the other valves during the testing in regards to flow.

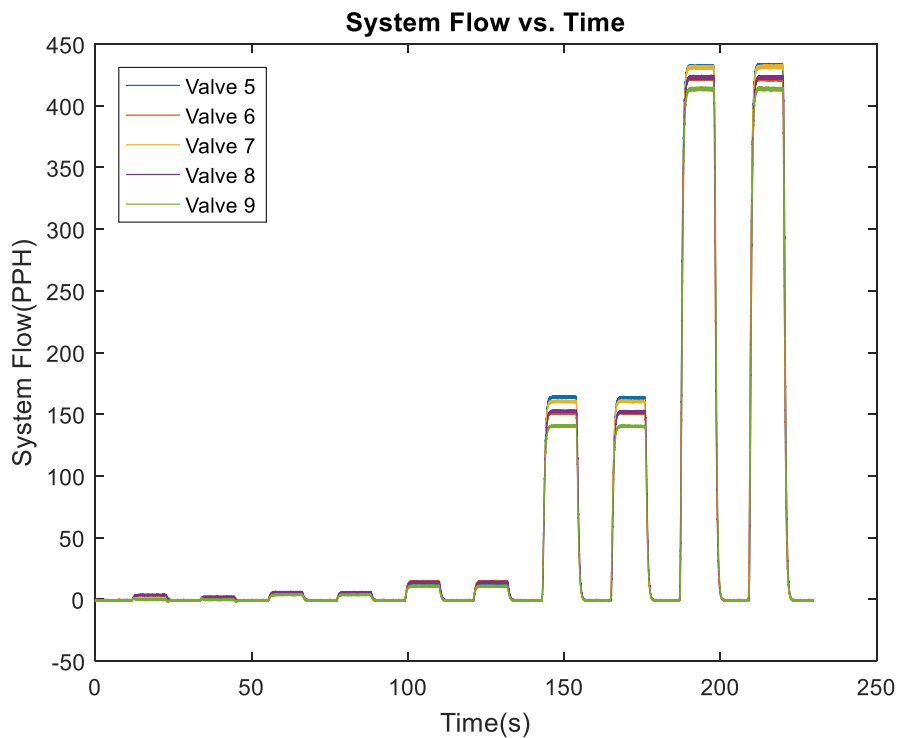


Figure 43: All FDV's flow data collected with test stand from the High Impulse Testing program.

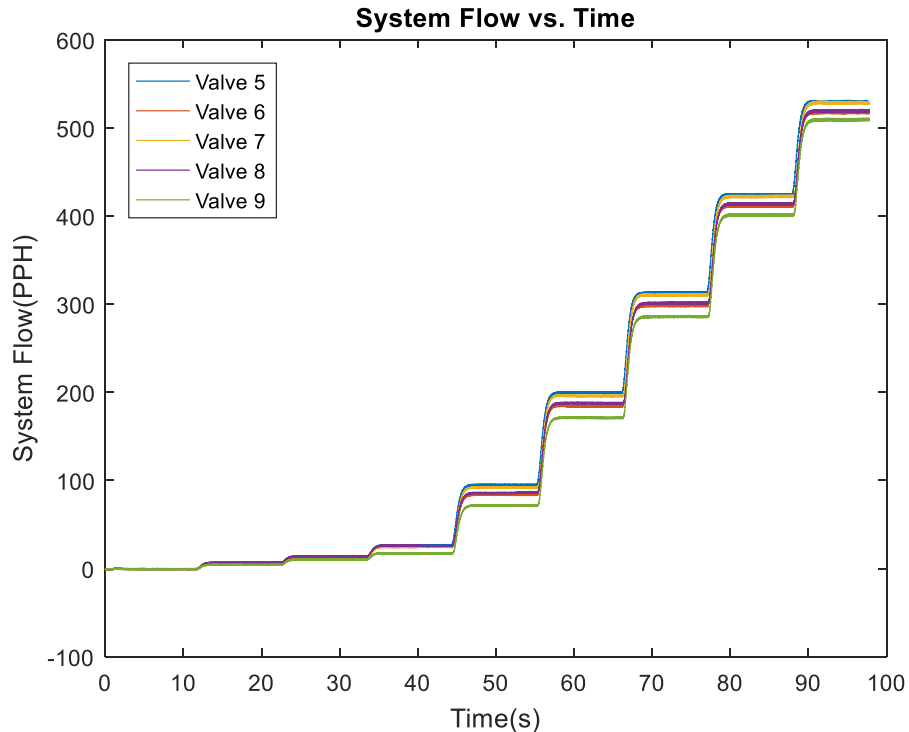


Figure 44: All FDV's flow data collected with test stand from the Continuous Step Testing program.

The check valve data collection failed overall. While the fixturing and pressure transducers worked well for data collection, the optical sensor failed to collect any useful data. However, this was not due to cavitation interference. During the calibration of the optical sensor, it was clear that the system setup that was designed and worked relatively successfully for the FDV was not going to be able to be implemented for the CV. Calibration attempts resulted in a voltage readout that did not correlate at all to the movement of the check valve via. drop gage. Therefore, there is no calibration data or fixture FN data to report on. After it was clear that the optical sensor would not work, data collection efforts for the CV had to be abandoned.

There are a few suspected flaws with the system setup for the CV that can be assumed to have caused the failure of the optical sensor reading. One is that the mirrored surface of the CV was not entirely adequate or consistent enough for the optical sensor. The mirrored surface of the CV system was a machined and polished surface. It's possible the machined surface did not provide enough reflection or a consistent enough reflection to allow accurate readings. Further testing of the optical probe would have to be done to know certainly. The other suspected issue was that the inlet for check valve, which was the path of the optical sensor, was slightly smaller than the tip of the optical sensor itself. As seen in Fig. 34 in Section 4.6, the flow channel is small and potentially in the way of the sensor optical beam. The channel size upstream from the check valve mirror may have been a contributing issue. The inlet hole size for the CV is $0.1285'' \pm .0005''$ while the optical sensor fiber is $0.187''$. This wasn't established as a potential issue until calibration of the CV was done.

5.2 Simulation

Relatively simple simulation work was done prior to introducing the experimental data. These simulations were run to ensure the simulation was behaving as expected. Generally, the simulations used nominal valve characteristics for the variables that were later honed during optimization work. If adjustments needed to be made to the model, the simulation variables were modified in an attempt to match AATech production test expectations.

FDV simulation was done to ensure simulation function, but also as a way to compare simulation output with regards to empirically collected valve characteristic data. Fig. 45 and Fig. 46 show a comparison of each valve's performance relative to stroke and flow respectively. The only variable data in this simulation was the measurable valve qualities of each valve. Those variables include spring rate, valve geometry, and valve masses.

The other variables in the simulation, which were the target of the optimization function were set to reasonable approximations. Spring preload was set at 11 lbs/in², damping coefficient at 0.4, pressure area at 0.19 in², coefficient of discharge of the system at 0.35, and eccentricity factor at 2.5. The pressure input was simulated using a simple signal generator in Simulink as shown in Fig. 22 in Section 4.4. The signal generated stepped the valves through pressures 0PSI-60PSI-80PSI-125PSI-150PSI-225PSI-0PSI with step input signal increase. Pressure was changed every 5 seconds in the plot. The instant step input signal increase coupled with the damping coefficient selected is most likely the reason for the high overshoot of valve stroke at pressure step points in the simulation plots in Fig. 45 and Fig. 46.

All valves' behavior matched with the other valves which is expected for a high production and high precision aerospace valve. All valves performed as expected with regards to stroke and valve flow.

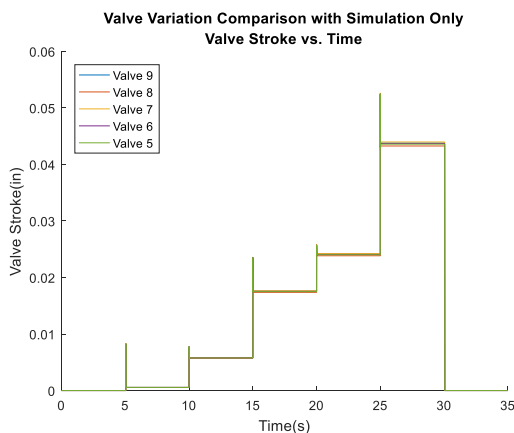


Figure 45: Plot comparing all valves stroke response with the only variables being the empirically collected measurements of the valves. Simple pressure signal input used in Simulink.

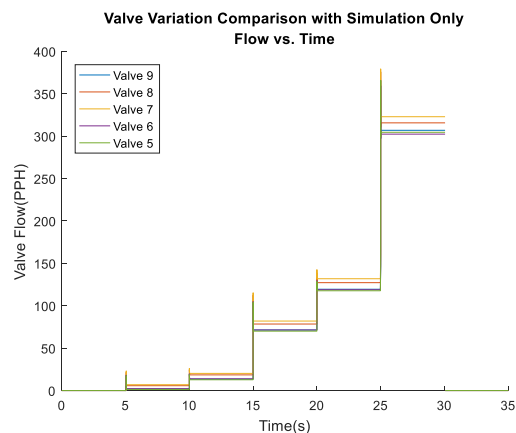


Figure 46: Plot comparing all valves flow with the only variables being the empirically collected measurements of the valves. Simple pressure signal input used in Simulink.

CV simulation was done with a focus on creating a system that output the same results as the production hardware was expected to. The simulation tested specific pressure points that would be tested in production hardware. No variable comparison was done for this simulation as there was no need to show how the different valves behave. All geometric, spring rate, and mass data for this simulation were taken from hardware nominal values. Spring preload, coefficient of discharge, and damping ratio were set and modified in order to create a simulation that matches production flow check expectations.

Spring preload was set at 0.2 lb/in², damping coefficient at 10, and coefficient of discharge at 0.01. The need for an exceptionally low coefficient of discharge can be attributed to the fact that the flow simulation for this system relied on only one pressure drop, while the production flow test setup and requirements, that the simulation was being matched too, involve several linear pressure drops. None of the production test setup pressure drops were included in the simulation, and therefore all pressure drop simulation of the system is effectively being accounted for in the frustum flow calculation. The coefficient of discharge must be exceptionally low to take all the system pressure drops into account through one area.

The pressure input was simulated using a simple signal generator in Simulink as shown in Fig. 22 in Section 4.4. The signal generated stepped the valves through pressures 0PSI-15PSI-25PSI-35PSI-70PSI-10PSI-0PSI with step input signal increase. Pressure was changed every 5 seconds in the signal.

The simulation matched production expectation almost perfectly and the pressure profile also allowed for the simulation to show the effects of overbalance on this CV. From 25-30 seconds it's clear that the overbalance effect is in play. A comparison of how the valve behaved at 15PSI at times 5-10 seconds shows that the valve did not open until it 25PSI was applied to the system, while it stayed open with only 10PSI at the 25-30 seconds time frame. This shows the modeling technique used in the research effectively models the CV and its overbalance effect. There is no more work done on the CV after this section.

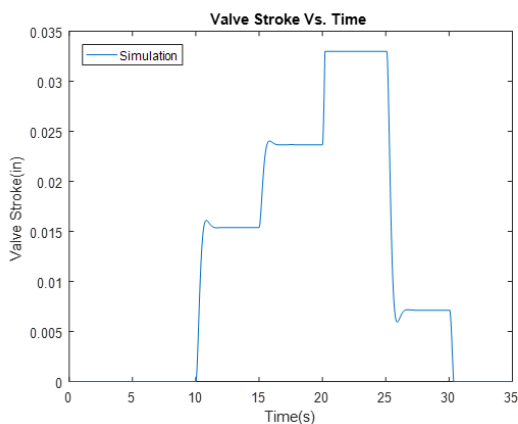


Figure 47: CV simulated stroke results with near production test points.

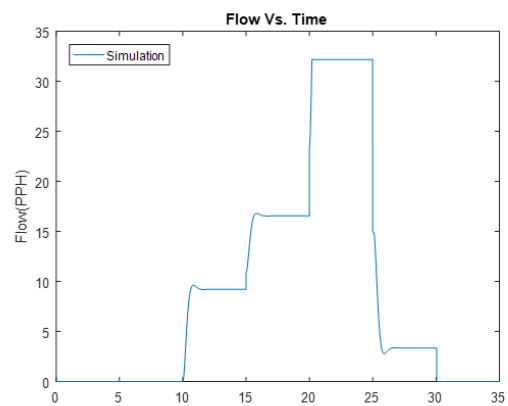


Figure 48: CV simulated flow results with near production test points.

5.3 Cost Analysis Optimization with Transient Data

Optimization of the FDV simulations was attempted in two stages. The first stage of optimization was done on the valve stroke simulation with the experimental data set collected from the Dewesoft and associated system of sensors. This was done first due to the reliance of the flow calculation on the stroke output. The second stage of optimization was done on the flow calculation via. comparison to the flow data from the test stand and associated system of sensors.

Cost analysis optimization was done for each valve in regard to the stroke. The variables that were run through the cost analysis were the spring preload, pressure area, and damping coefficient. The optimized values as found by the “fminsearch” function in MATAB with a cost analysis evaluation are shown in Table 5 as well as the cost value that was last output for the simulation.

Cost Analysis Optimization of FDV					
Valve #	5	6	7	8	9
Spring Preload	10.7295	10.9794	10.8082	10.8793	11.0089
Pressure Area	.2384	.2306	.2370	.2349	.2316
Damping Coef.	.3683	.3736	.3710	.3733	.3757
Cost for Stroke	3.7017e-04	7.3837e-04	4.7931e-04	6.0347e-04	6.4624e-04

Table 5: FDV properties as generated with an RMS cost analysis of the simulation and experimental data.

Fig. 49 shows the cost analysis values for the optimization of Valve 7 for the variable associated with the stroke of the valve. The figure is representative of all of the valves optimization attempts. All yielded converging optimization solutions like the one shown in Fig. 49.

Figure 49: Cost Value of an optimization attempt made on Valve 7 simulation, Continuous Step Increase program.

Even though optimization resulted in a convergent solution that yielded a low cost value, the optimization did not work. Fig. 50 – 54 show how the optimized variable values performed during simulation. Fig. 50 – 54 show all 5 valves stroke simulation compared to their experimental data. There is a poor correlation between the two in every case.

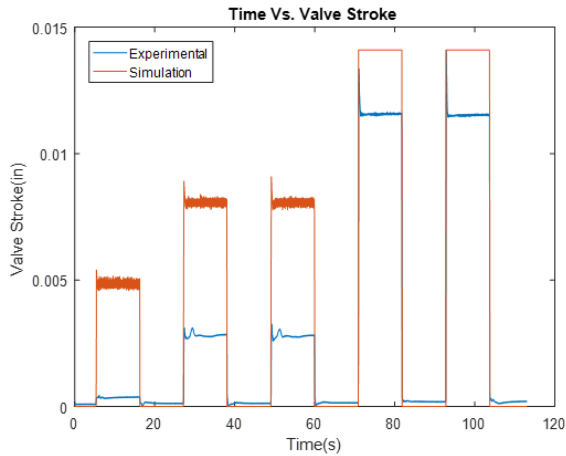


Figure 50: Valve 5 simulation with cost analysis optimized values

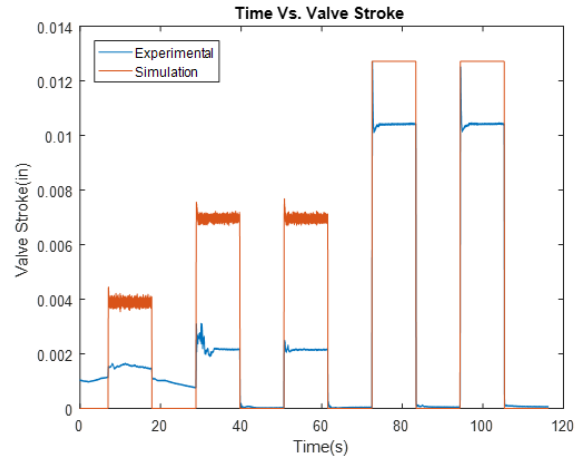


Figure 51: Valve 6 simulation with cost analysis optimized values

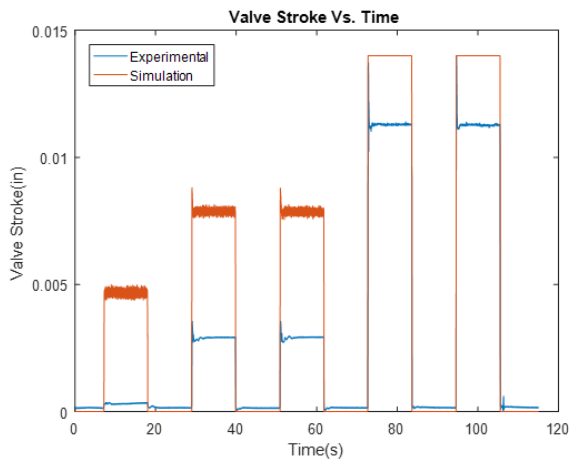


Figure 52: Valve 7 simulation with cost analysis optimized values

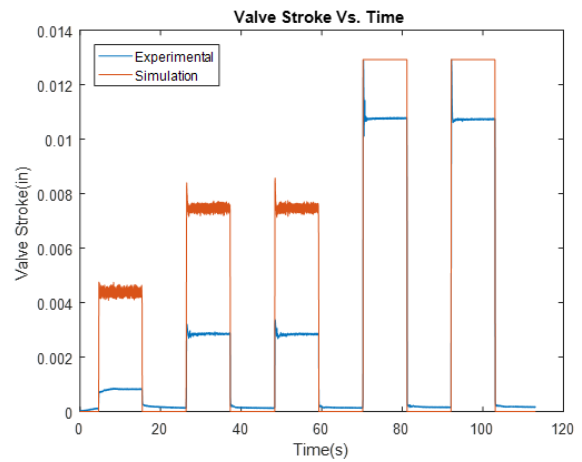


Figure 53: Valve 8 simulation with cost analysis optimized values

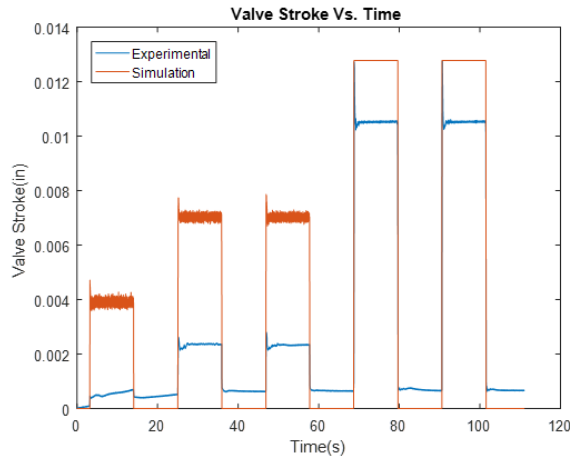


Figure 54: Valve 9 simulation with cost analysis optimized values

There are a couple theories that were generated to explain the failure of the optimization. One problem that can arise with the MATLAB “fminsearch” function is that the initial variable setup can cause a failure to converge properly. This happens because the function ends up checking too narrow of a window in regards to variables and finds a minimum cost function within that narrow window. The setup variables were adjusted several times in order to trial this potential problem. In all cases, the optimization code always returned the variables to the values shown in Table 5. Another possibility is that the data is so irregular due to the cavitation effects that the “fminsearch” has found the best fit that includes all the stray data in the experimental work. This problem was not solved in this thesis and would need further investigation. Instead, the valve stroke simulations were manually optimized which is explained in Section 5.4.

Cost analysis based optimization was also performed for the flow calculation of the FDV. The flows for the cost analysis calculations were taken with the test stand sensors. Unfortunately, none of the optimization attempts yielded a convergent solution. All attempts failed. This is most likely caused by the fact that the stroke optimization was less than ideal and the flow calculation and optimization relied on the valve stroke to function. It’s also possible that the flow area calculation is not as effective as it needs to be for this type of simulation and optimization. The flow slot area calculator is derived from a proprietary AATech tool and was not proven to match reality in this report. If the area calculation is not accurate for the entire range of valve stroke possible, then it may have impeded the optimization attempts.

It should be noted that the valve stroke manual optimization yielded much better results than the cost analysis based optimization. The most accurate optimization work was done on Valve 7 and is covered more in Section 5.4. However, it should be noted in this section that even when using Valve 7 optimization results, the cost analysis optimization for Valve 7 flow failed to converge.

5.4 Manual Optimization

As mentioned in the previous section of this report, the cost analysis based optimization attempts had poor correlation for valve stroke, and failed to converge to a solution for valve flow for the FDV. Due to this fact, the simulations had to be manually optimized. This was an extensively iterative endeavor but yielded much better results than the MATLAB “fminsearch” function for this specific setup.

In order to gage the iterative steps to take and the starting points for the manual optimization of the valve stroke simulation, the simulation was evaluated through varying each characteristic of interest for optimization individually and assessing the impact of that variance on the stroke output. A representative of these results of these attempts to evaluate effect of the variables on stroke are shown in Fig. 55 – 57. These plots were all done specifically for Valve 7, although the rest of the valves obviously performed nearly identically. In the figures, the simulation results are compared to the experimental data.

Fig. 55 shows variation in the pressure area from 0.21 in² to 0.17 in² in increments of 0.01 in². “data5” is the stroke simulation of pressure area 0.17 in² and “data1” is the stroke simulation of pressure area 0.21 in². Fig. 56 shows the effect of a spread of damping coefficients. This plot shows one small section of the plot in order to help show the different simulations since they are overlapping in many areas. The damping coefficient was varied from 0.4 to 0 in 0.1 increments. There is no visually discernable difference between the simulations. “data5” in Fig. 56 is the 0.4 damping coefficient while “data1” is 0. Fig. 57 shows variation in the spring preload from 13 lb/in² to 9 lb/in² in 1 lb/in² increments. “data5” is the 13 lb/in² preload while “data1” is the 9 lb/in² preload.

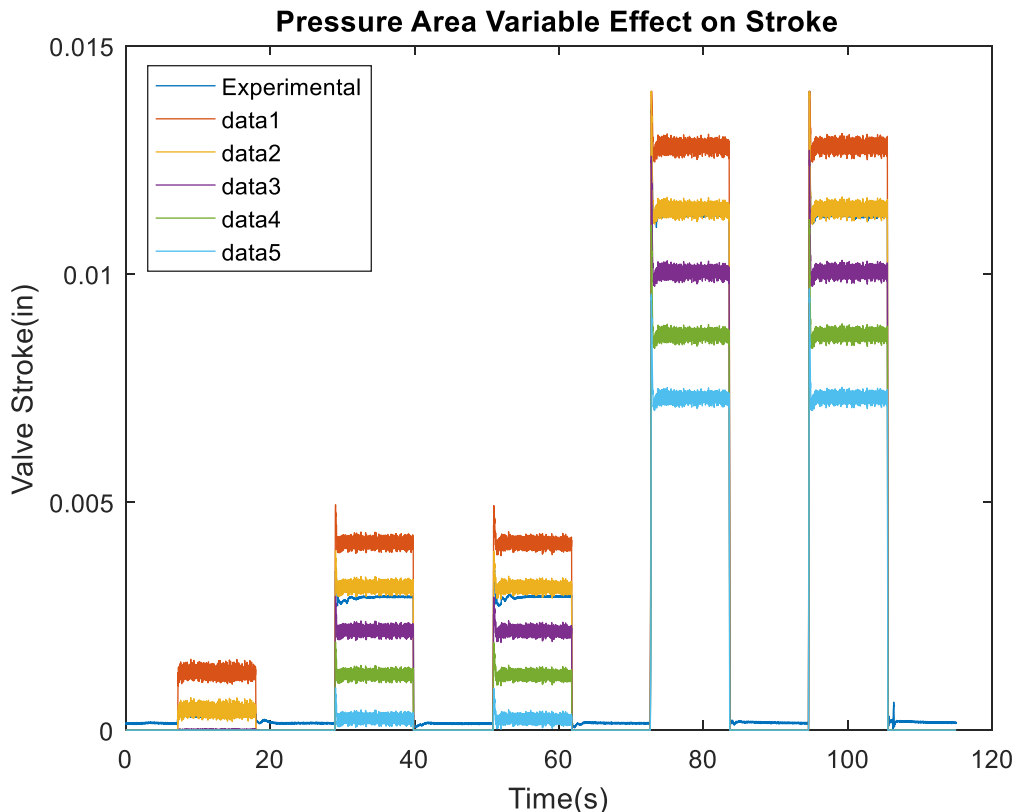


Figure 55: Plot showing the effects of varying the pressure area variable on the stroke of Valve 7

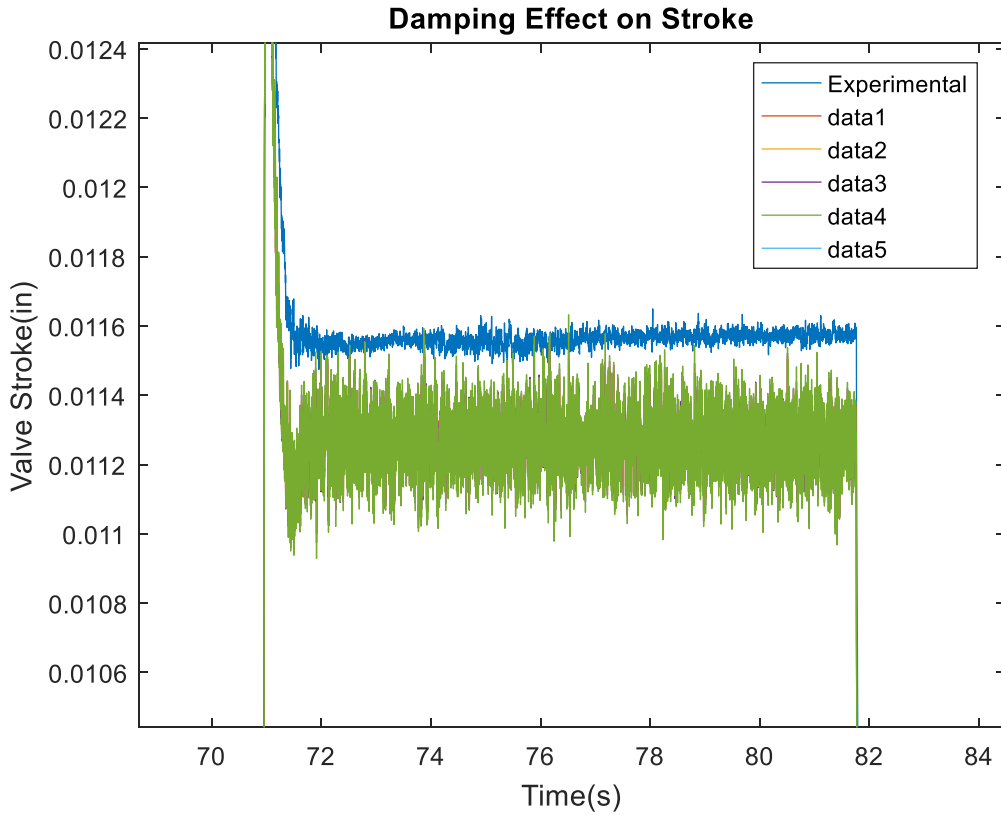


Figure 56: Plot showing the effects of varying the damping ratio variable on the stroke of Valve 7.

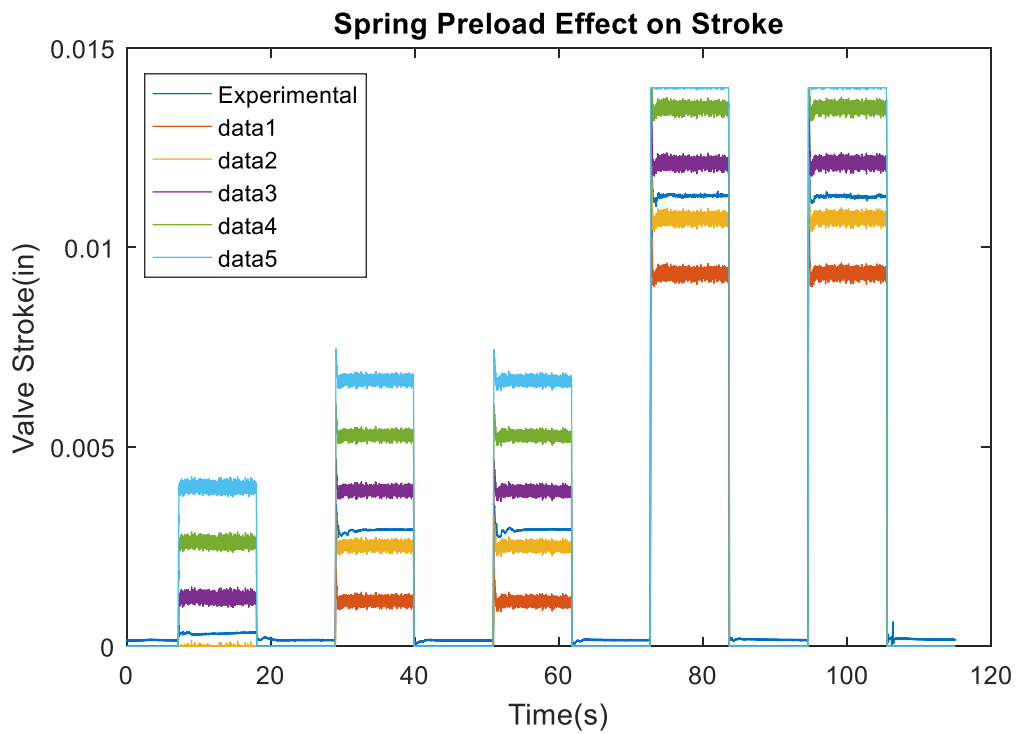


Figure 57: Plot showing the effects of varying the spring preload variable on the stroke of Valve 7.

Through an iterative process, much like what the “fminsearch” function performs, and through visual comparison of simulation results to experimental results, the best fit variables were eventually identified. Due to this process being based on a visual optimization and some assumptions about valve stroke having to be made due to the effects of cavitation, the variables may contain a degree of error.

Fig. 58, Fig. 60, Fig. 62, Fig. 64 and Fig. 66 all show the results of the manual optimization efforts for Valve 5, Valve 6, Valve 7, Valve 8, and Valve 9 respectively. The variables that were adjusted to match simulation and experimental data were spring preload, pressure area, and damping coefficient. The final variables are shown in Table 6 at the end of this section. The variables were manually adjusted to match the simulation and experimental data for the High Impulse Test program. Those manually optimized values were then used in a comparison trial to see if they would result in accurate performance of the simulation using another test program. The Continuous Step Increase Test program was used as a comparison base and the results of that comparison are seen in Fig. 59, Fig. 61, Fig. 63, Fig. 65 and Fig. 67 for Valve 5, Valve 6, Valve 7, Valve 8, and Valve 9 respectively.

The valves all matched well with simulation. They also showed good matched results in the comparison work against the other test program. Results of the manual optimization of the valve stroke were substantially better than the cost analysis optimization attempts.

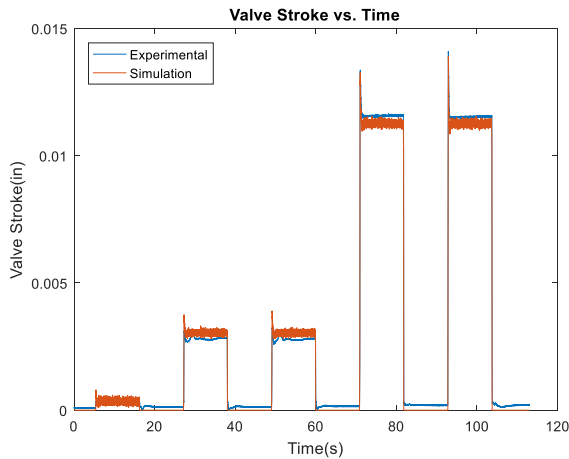


Figure 58: Valve 5 simulation manually corrected to match reality

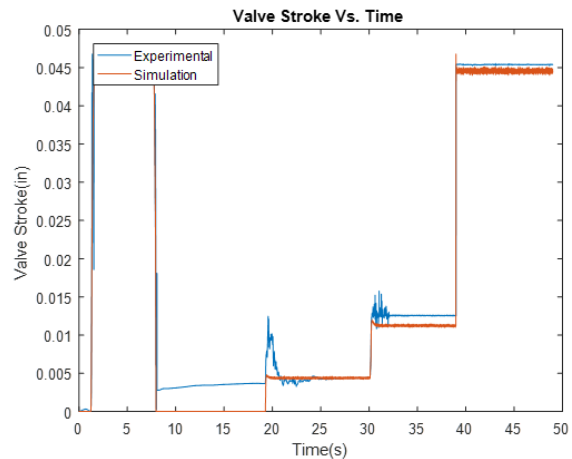


Figure 59: Valve 5 corrected variables compared to other program

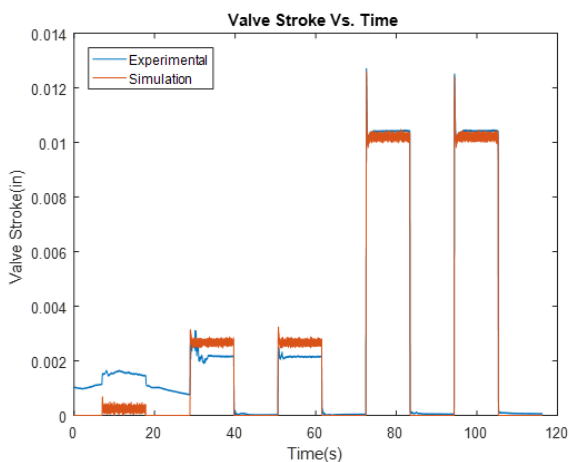


Figure 60: Valve 6 simulation manually corrected to match reality

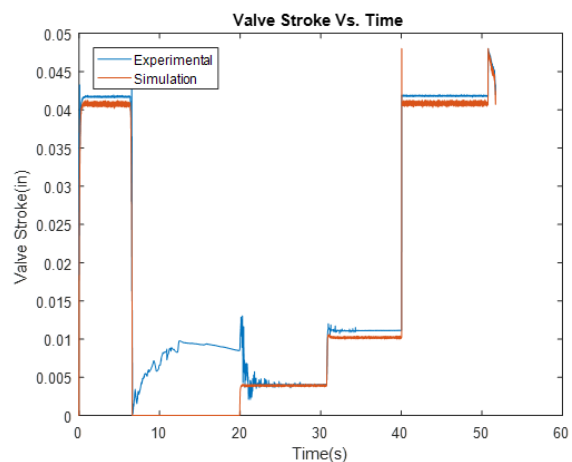


Figure 61: Valve 6 corrected variables compared to other program

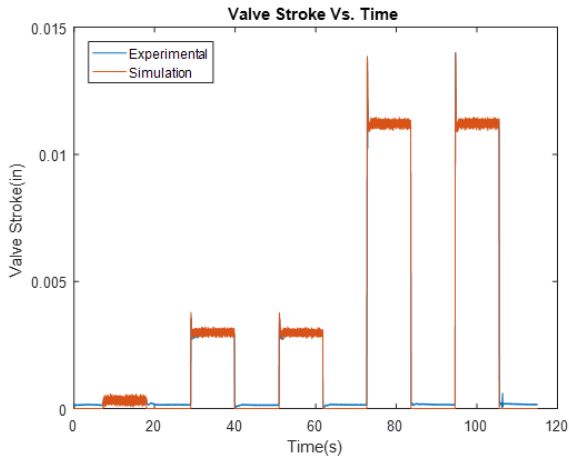


Figure 62: Valve 7 simulation manually corrected to match reality

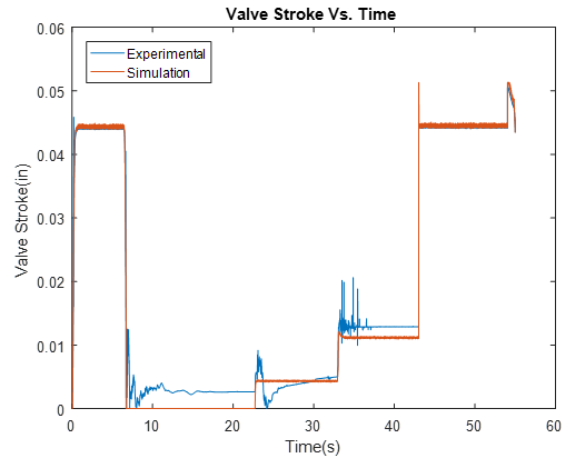


Figure 63: Valve 7 corrected variables compared to other program

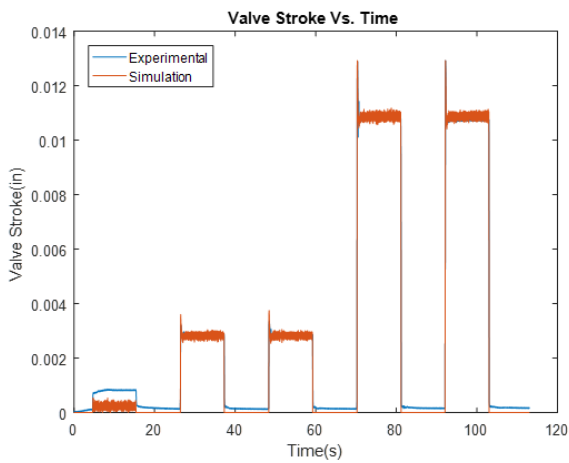


Figure 64: Valve 8 simulation manually corrected to match reality

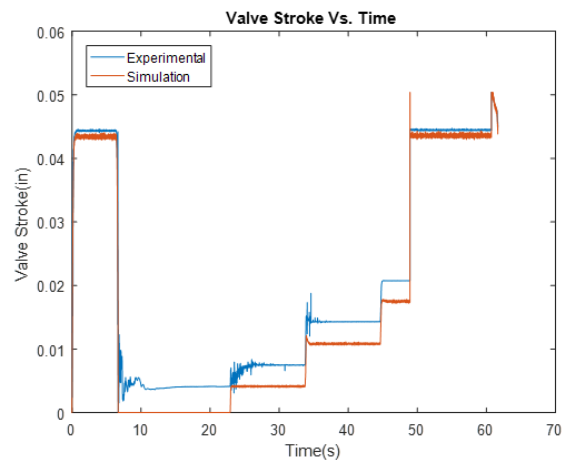


Figure 65: Valve 8 corrected variables compared to other program

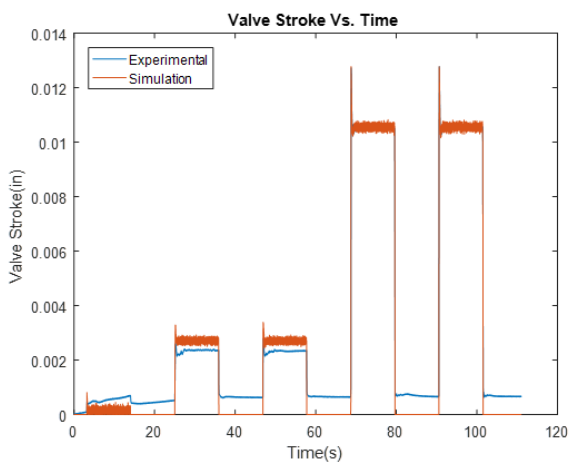


Figure 66: Valve 9 simulation manually corrected to match reality

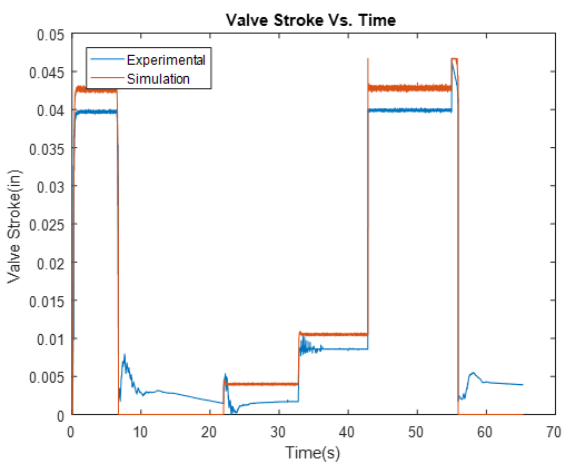


Figure 67: Valve 9 corrected variables compared to other program

In the same manner as the valve stroke manual optimization, the flow calculation manual optimization was initialized by creating plots with specific variables plotted across a range of values. In this case, the coefficient of discharge and the eccentricity were plotted over a range of values. A representative of these results of attempts to evaluate effect of variables on valve flow are shown in Fig. 68 and Fig. 69 which show variation of coefficient of discharge and eccentricity respectively. These plots were created using Valve 7 experimental data and simulation matrix.

Fig. 68 shows variation in the coefficient of discharge from 0.25 to 0.45 in increments of .05. “data5” is the flow simulation of a discharge coefficient of 0.45 and “data1” is the stroke simulation of a discharge coefficient of 0.25. Fig. 69 shows the effect of variation in the eccentricity for the bleed flow calculation with a value of 2.5 to 0.5 in increments of 0.5. “data5” represents the eccentricity value of 2.5 and “data1” represents the eccentricity values of 0.5.

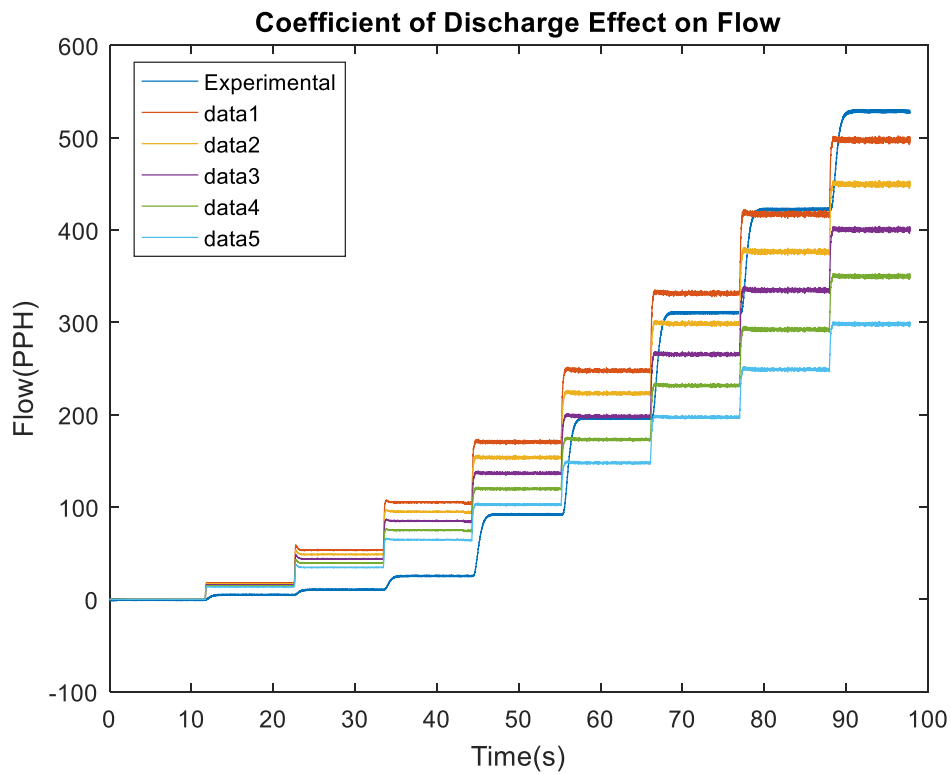


Figure 68: Plot showing the effects of varying the coefficient of discharge variable on the flow of Valve 7.

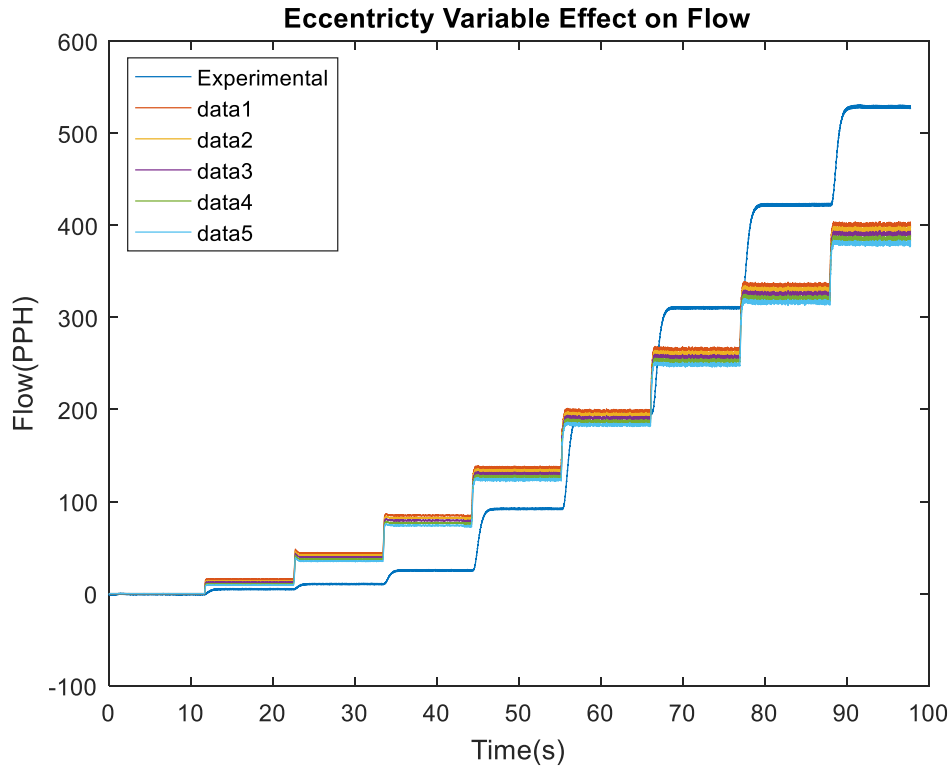


Figure 69: Plot showing the effects of varying eccentricity variable on the flow of Valve 7.

Once again, through the same process as was done with the manual optimization of the valve stroke, the best fit variables were eventually identified for the flow calculation for each valve. The fit of the plots was not as exact as with the valve stroke. The flow calculation does not track well with the simulation. This suggests that the area calculation is the culprit in the failure to use cost analysis optimization for the flow simulation.

Fig. 70, Fig. 72, Fig. 74, Fig. 76 and Fig. 78 all show the results of the manual optimization efforts for Valve 5, Valve 6, Valve 7, Valve 8, and Valve 9 respectively. The variables that were adjusted to match simulation and experimental data were coefficient of discharge and eccentricity of bleed. The final variables are shown in Table 6 at the end of this section. The variables were manually adjusted to match the simulation and experimental data for the Continuous Step Increase Test program. Those manually optimized values were then used in a comparison trial to see if they would result in accurate performance of the simulation using another test program. The High Impulse Test program was used as a comparison base and the results of that comparison are seen in Fig. 71, Fig. 73, Fig. 75, Fig. 77 and Fig. 79 for Valve 5, Valve 6, Valve 7, Valve 8, and Valve 9 respectively.

Valve simulations matched reasonably well for some mid-range test pressures but did not match well overall. The flow did not track with the experimentally collected data. The experimentally collected valve flows increased in a more exponential manner, while the simulated flows were more linear. The comparative plots done with the High Impulse Test program yielded similarly poor results.

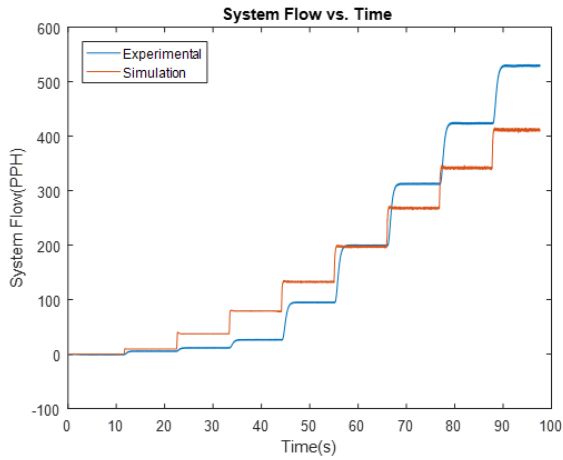


Figure 70: Valve 5 simulation manually corrected to match reality

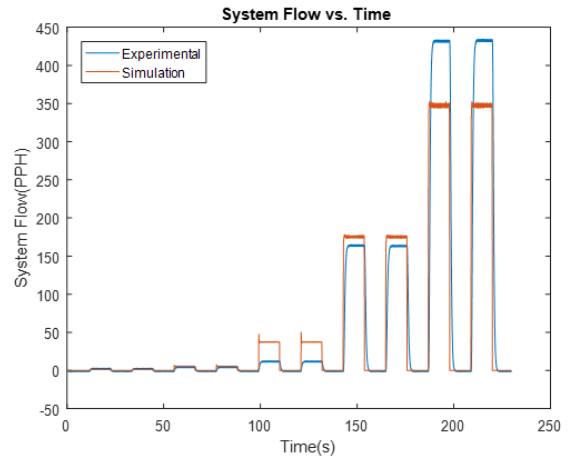


Figure 71: Valve 5 corrected variables compared to other program

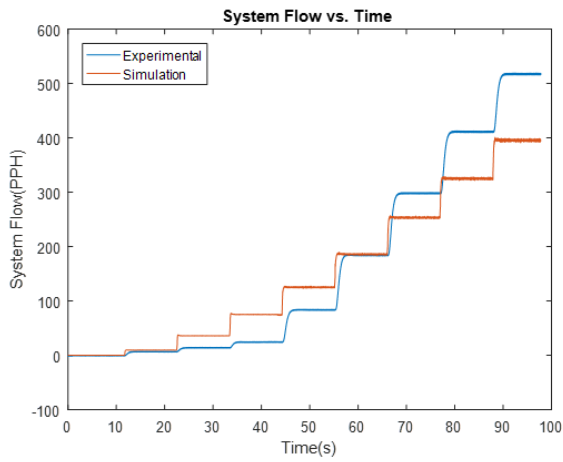


Figure 72: Valve 6 simulation manually corrected to match reality

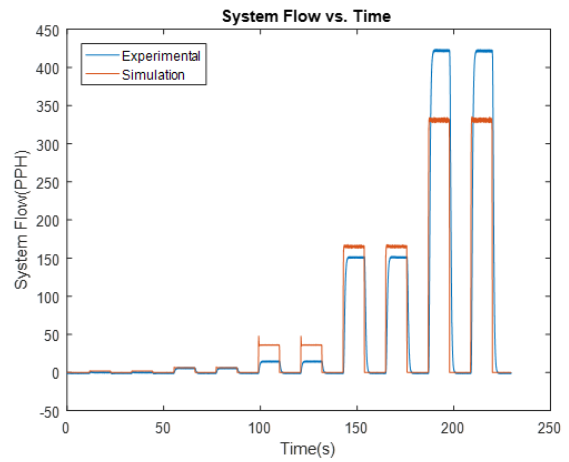


Figure 73: Valve 5 corrected variables compared to other program

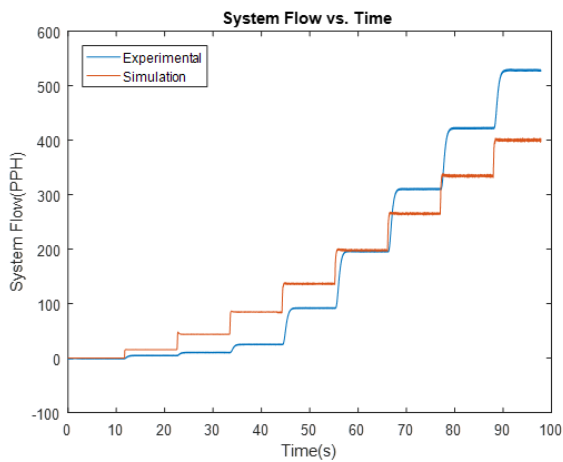


Figure 74: Valve 7 simulation manually corrected to match reality

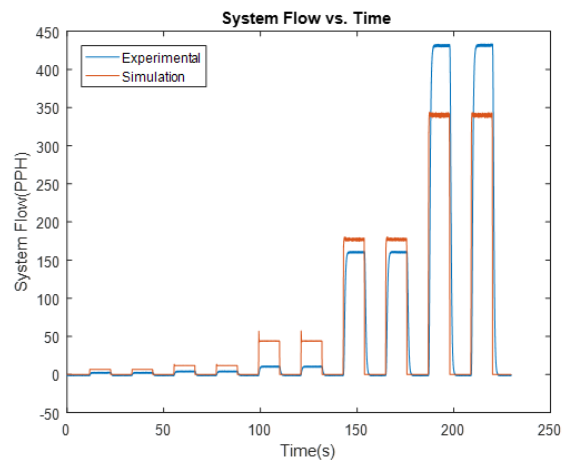


Figure 75: Valve 5 corrected variables compared to other program

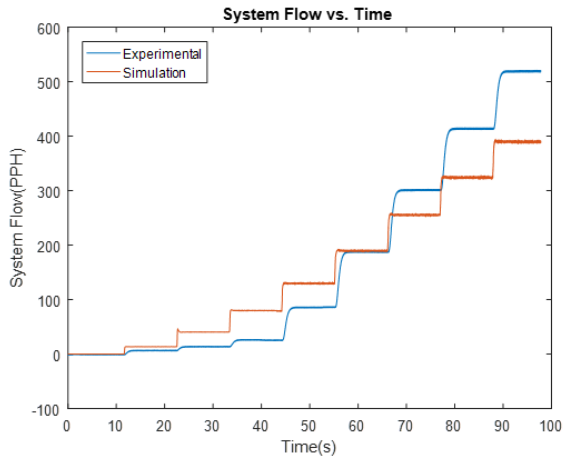


Figure 76: Valve 8 simulation manually corrected to match reality

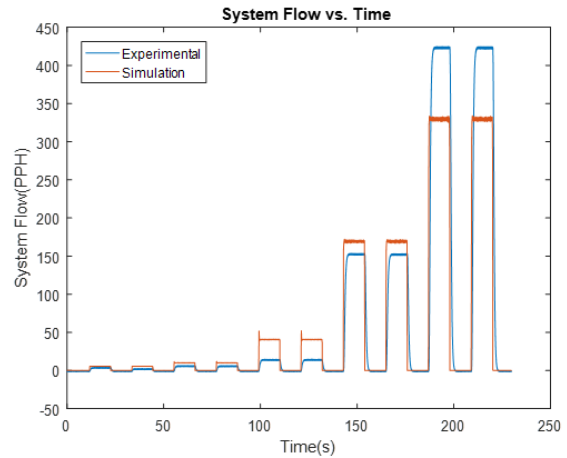


Figure 77: Valve 5 corrected variables compared to other program

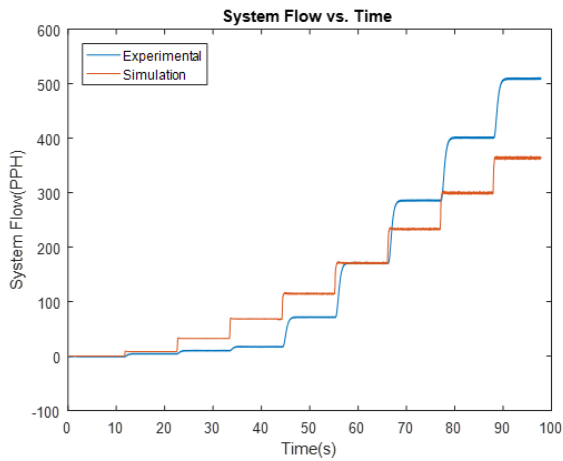


Figure 78: Valve 9 simulation manually corrected to match reality

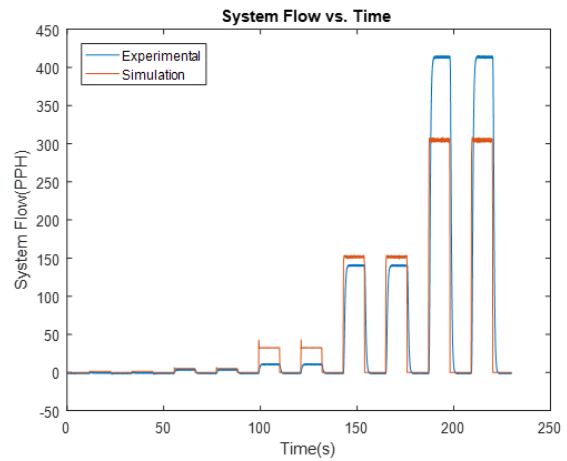


Figure 79: Valve 5 corrected variables compared to other program

Manual Optimization Results					
Valve #	5	6	7	8	9
Spring Preload	11.75	10.75	11.65	11.65	11.25
Pressure Area	.2005	.1825	.1985	.1970	.1900
Damping Coef.	.3683	.3736	.3710	.3733	.3757
Cd	.375	.4	.35	.35	.345
Bleed Eccentricity	2.5	2.5	2.5	2.5	2.5

Table 6: FDV properties as generated through manual comparison to experimental data.

5.5 Cost Analysis Optimization with Steady State Data

Due to the results yielded by the cost analysis optimization and the issues seen in the data collection due to cavitation, it was decided that a second optimization review should be done with the measurement data converted into steady state data points.

Steady state evaluation was done by taking 100 data points from each pressure set point during the test programs and averaging them to create one steady state point. This data point for each pressure set point of the test programs was applied to the valve calculation and the optimization setup to be optimized. The test program that was optimized against was the High Impulse Test Program for the valve stroke.

The results of the steady state optimization were similar to original optimization attempts. They yielded equally unsuccessful attempts at optimizing the variables in stroke and flow as the optimization of the entire data set. The stroke optimization showed a constantly decreasing cost value down to a convergent point. The cost value solution can be seen in Fig. 69 However, the optimization of the flow did not converge. The “fminsearch” function was not able to bring the cost value down.

Steady State Cost Analysis Optimization of FDV Stroke					
Valve #	5	6	7	8	9
Spring Preload	9.6206	11.5434	11.6301	10.9275	11.5479
Pressure Area	.2143	.2021	.2240	.2248	.2020
Cost for Stroke	2.7565e-04	2.4e-03	4.5041e-04	6.5855e-04	5.4667e-04

Table 7: Optimized stroke values as determined by the Cost Analysis optimization technique.

Fig. 80 shows the cost analysis values for the optimization of Valve 7 for the variable associated with the stroke of the valve. The figure is representative of all of the valves optimization attempts. All yielded converging optimization solutions like the one shown in Fig. 80.

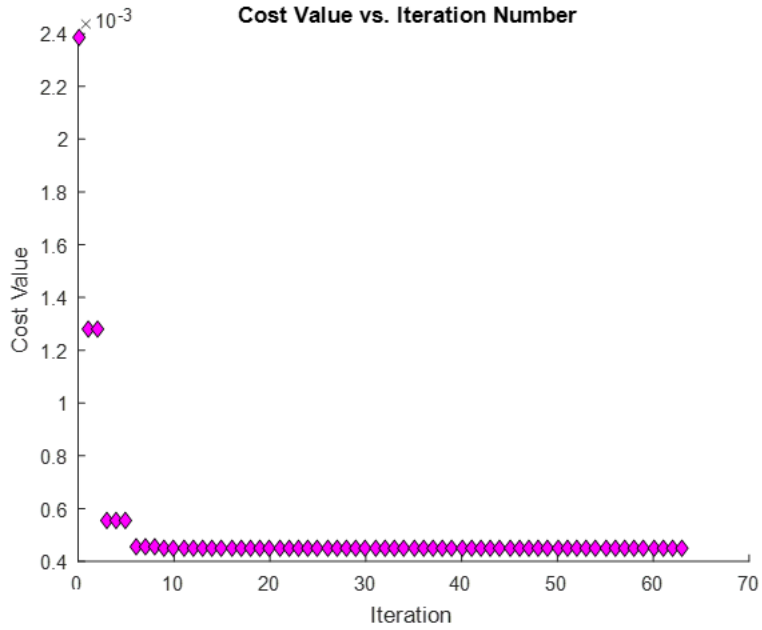


Figure 80: Plot of the cost value of each iteration of the “fminsearch” optimization

The values that the cost analysis optimization technique yielded were then used to generate steady state plots to show how closely the optimized values calculations compared to experiment. The comparison plots are shown in Fig. 81 – 85.

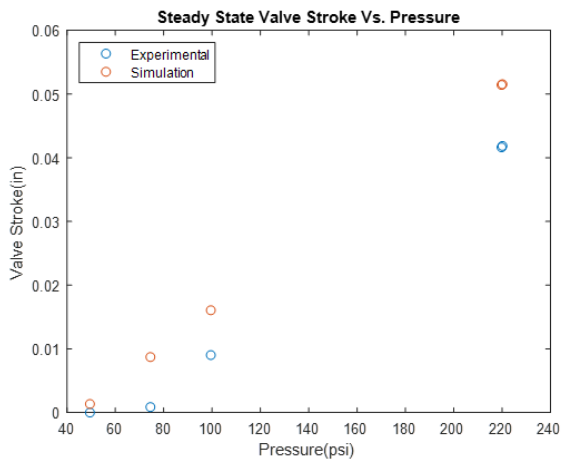


Figure 81: Valve 5 simulation with cost analysis optimized values

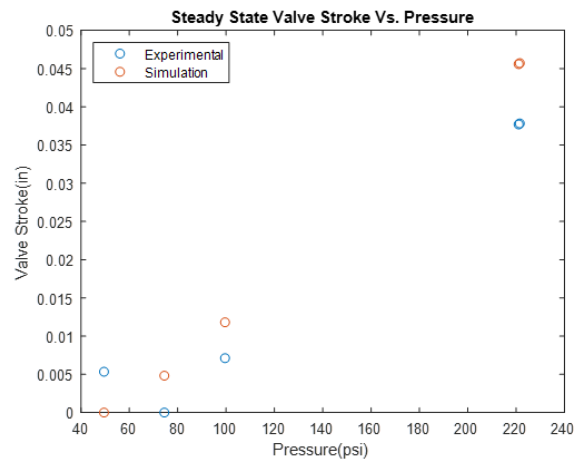


Figure 82: Valve 6 simulation with cost analysis optimized values

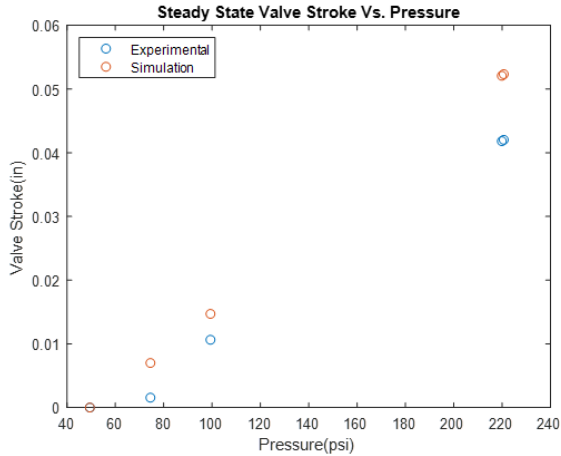


Figure 83: Valve 7 simulation with cost analysis optimized values

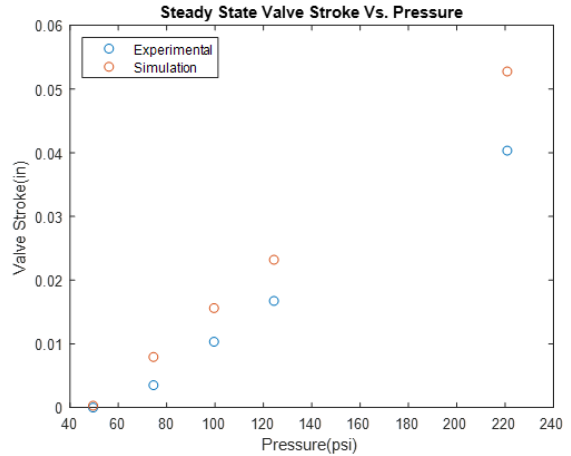


Figure 84: Valve 8 simulation with cost analysis optimized values

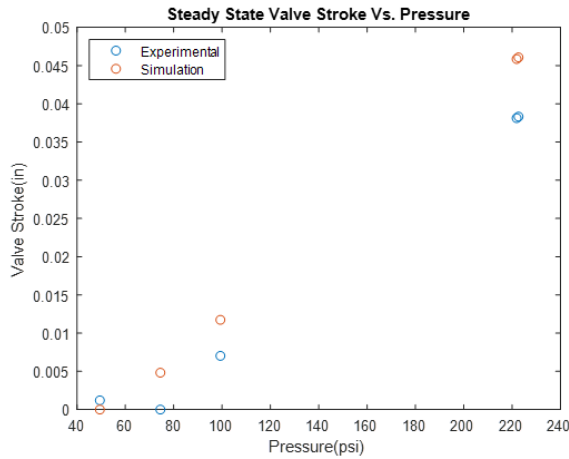


Figure 85: Valve 9 simulation with cost analysis optimized values

5.6 Uncertainty Analysis

The sources of uncertainty in this study were addressed and uncertainty propagation into the simulation was reviewed. This report touched on several of the topics of error throughout the results. There were several expected sources of error and some unexpected sources.

First, the uncertainty in the experimental sensors and data collection were evaluated. The uncertainty collected from the manufacturer of each sensor is shown in Table 8.

Sensor Error Data Summary			
Sensor System	Sensor Name	Data Type Collected	Uncertainty from Manufacturer Data
Dewesoft Data Acquisition	Kulite EXTEL-190	Pressure	+/- 2 PSI
	Philtec RC171	Displacement	+/- 0.00022 in
Test Stand Data Acquisition	GE Unik 5000	Pressure	+/- 4PSI
	Micromotion CMF	Fluid Flow	+/- .05% Rate of Flow

Table 8: Table of uncertainty data taken from manufactures technical data sheets.

Both systematic and random uncertainty were evaluated and combined to gage total uncertainty in the experimental data. The systematic uncertainty was evaluated using the manufacturer data that was shown in Table 8. The random uncertainty was evaluated by calculating the standard deviation of 100 data points from each pressure set point in the test programs. Systematic and random uncertainty were then combined using root sum square to achieve overall uncertainty data for each measurement. The root sum square uncertainty calculations are shown in Eq. 27.

$$\delta T = \sqrt{(\delta S)^2 + (\delta R)^2} \quad (27)$$

In Eq. 27, δT represents the total uncertainty, δS represents systematic uncertainty, and δR represents the random uncertainty. These equations were applied to the sensors used in the experimental data collection.

Once total uncertainty was known for experimental data collection, the uncertainty was propagated through to the stroke calculation and the flow calculation for the steady state data points. This was done through a Monte Carlo simulation. The total uncertainty values calculated for the empirical data collection were used to generate 1000 data points for each experimental pressure set point. Those 1000 point data sets were then run through the valve calculations. The output of each of the 1000 point data set calculation had the standard deviation from each pressure set point calculated. That standard deviation was taken as the error of the calculated value. This was done for the valve stroke calculation and for the flow calculation.

The results of these uncertainty calculations can be seen in Fig. 86 - 105. Due to the fact that the manually optimized vales matched the experiment better than the cost analysis optimization in this research, the uncertainty propagation calculator used the manually acquired optimized values as seen in Table 6. Fig 86 - 95 show the results of the uncertainty bars on the stroke calculations for the High Impulse Test Program and the Continuous Step Test Program.

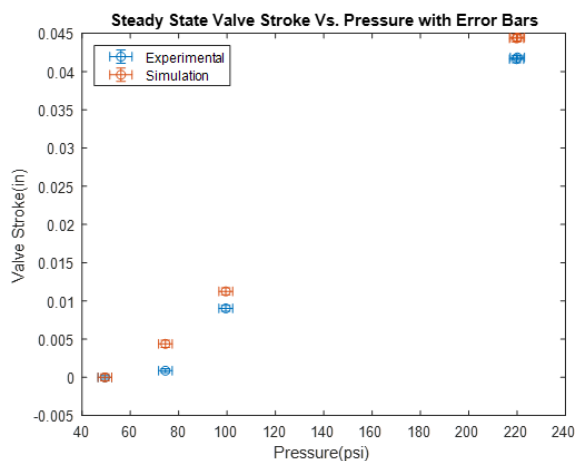


Figure 86: Valve 5 High Impulse Test Program stroke

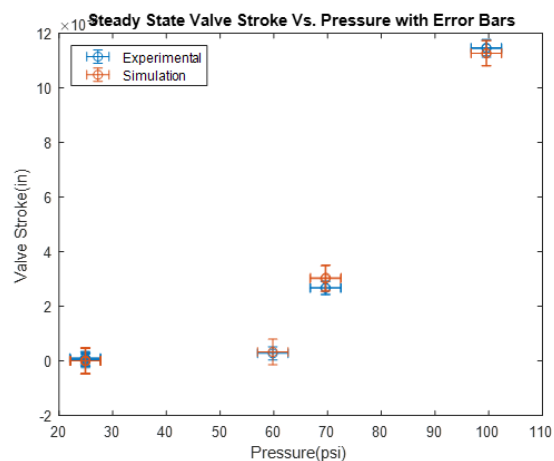


Figure 87: Valve 5 Continuous Step Test Program stroke

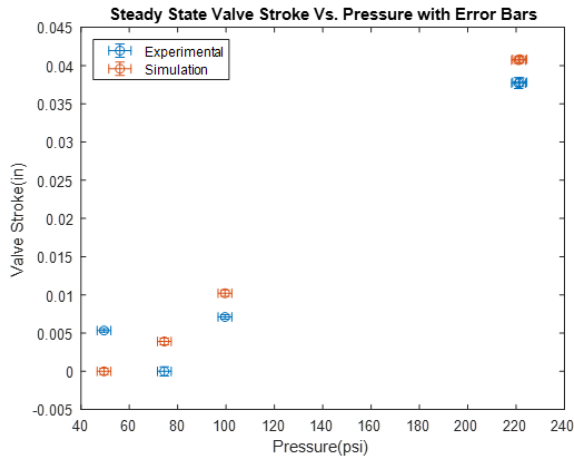


Figure 88: Valve 6 High Impulse Test Program stroke

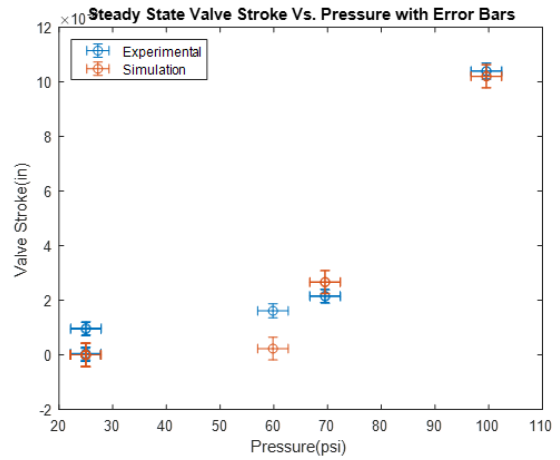


Figure 89: Valve 6 Continuous Step Test Program stroke

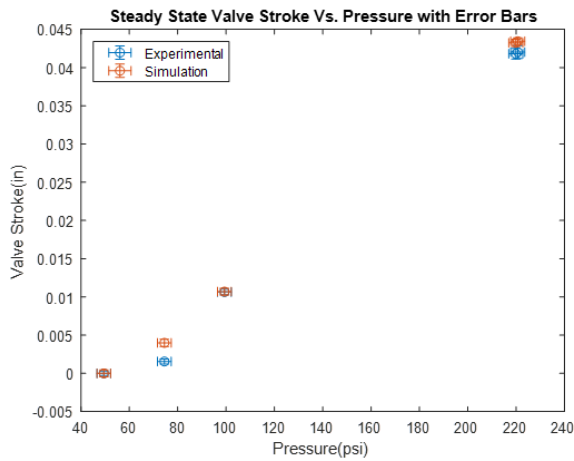


Figure 90: Valve 7 High Impulse Test Program stroke

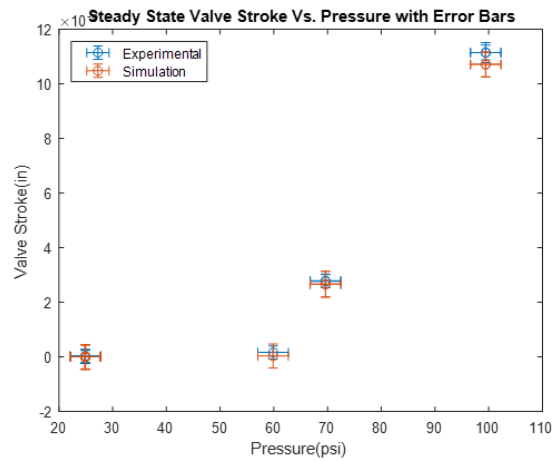


Figure 91: Valve 7 Continuous Step Test Program stroke

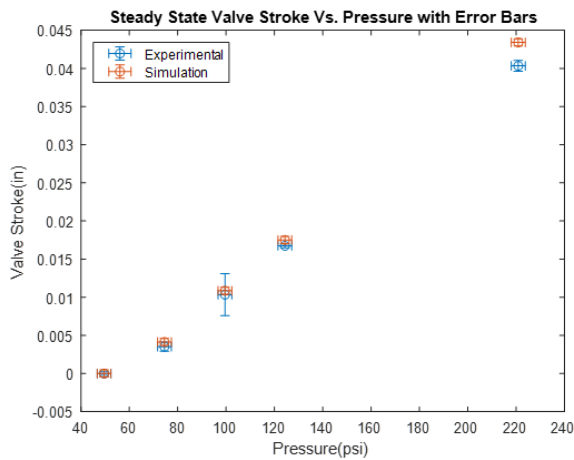


Figure 92: Valve 8 High Impulse Test Program stroke

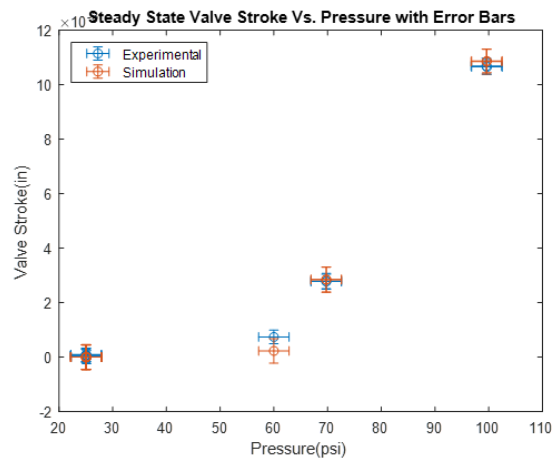


Figure 93: Valve 8 Continuous Step Test Program stroke

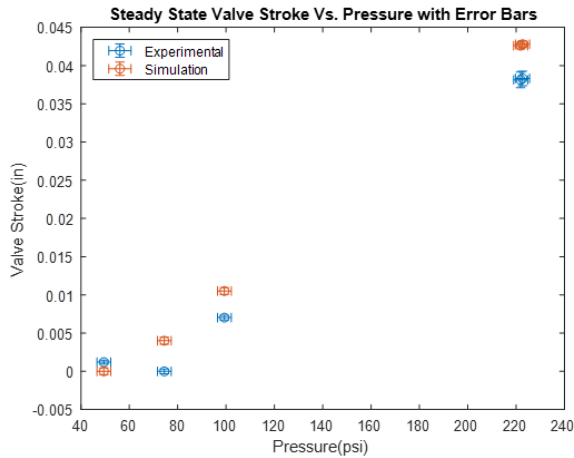


Figure 94: Valve 9 High Impulse Test Program stroke

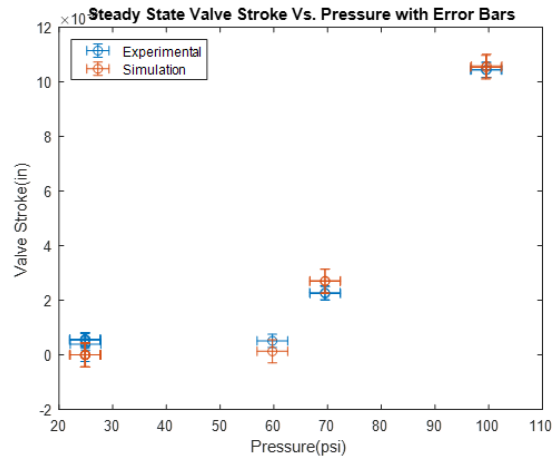


Figure 95: Valve 9 Continuous Step Test Program stroke

Fig. 96 - 105 show the results of the uncertainty bars on the flow calculations for the High Impulse Test Program and the Continuous Step Test Program.

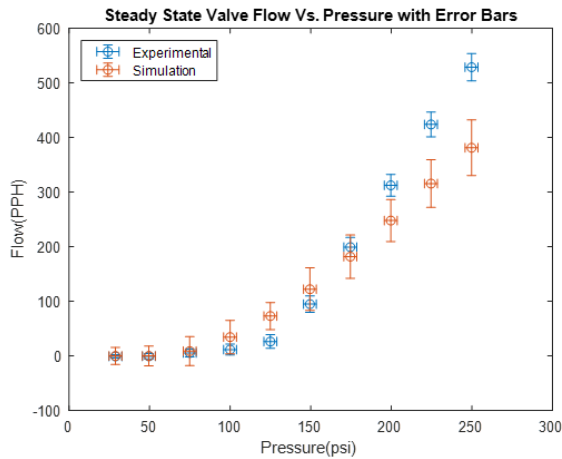


Figure 96: Valve 5 Continuous Step Test Program flow

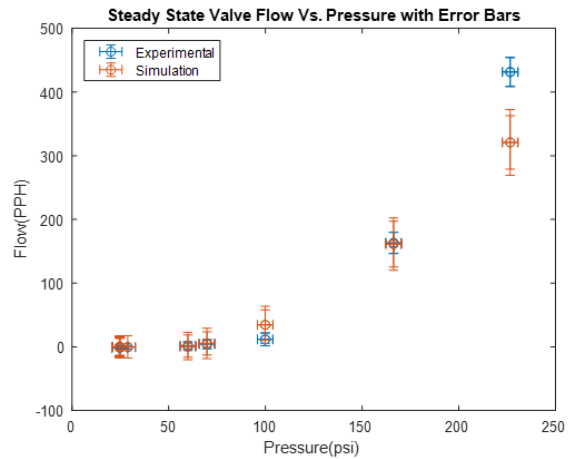


Figure 97: Valve 5 High Impulse Test Program flow

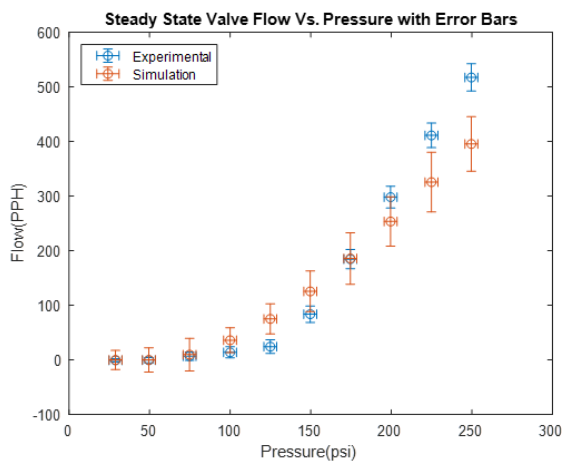


Figure 98: Valve 6 Continuous Step Test Program flow

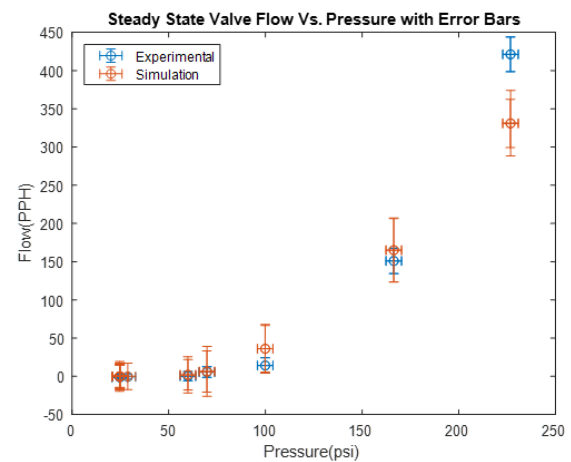


Figure 99: Valve 6 High Impulse Test Program flow

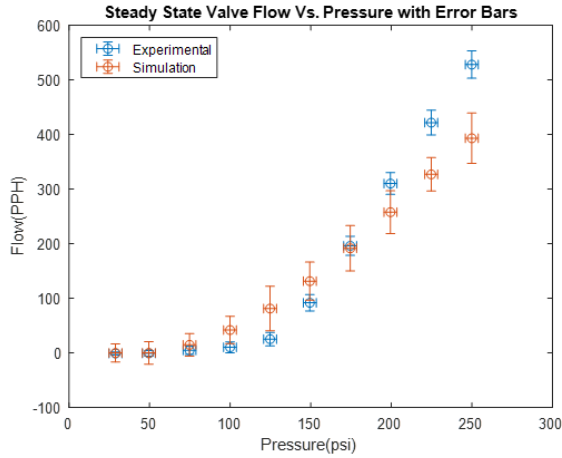


Figure 100: Valve 7 Continuous Step Test Program flow

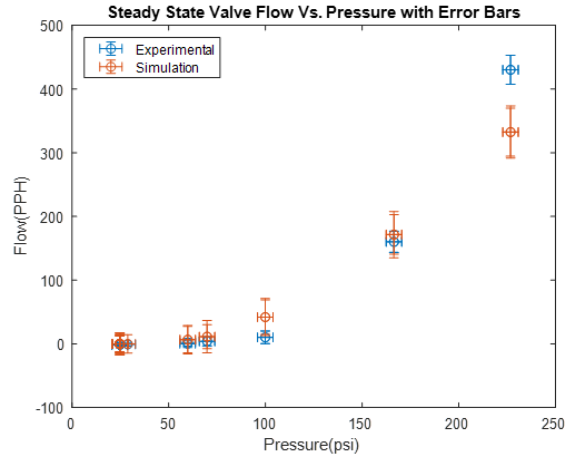


Figure 101: Valve 7 High Impulse Test Program flow

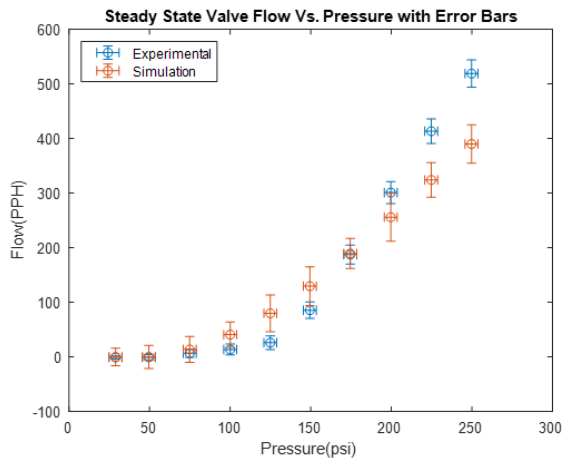


Figure 102: Valve 8 Continuous Step Test Program flow

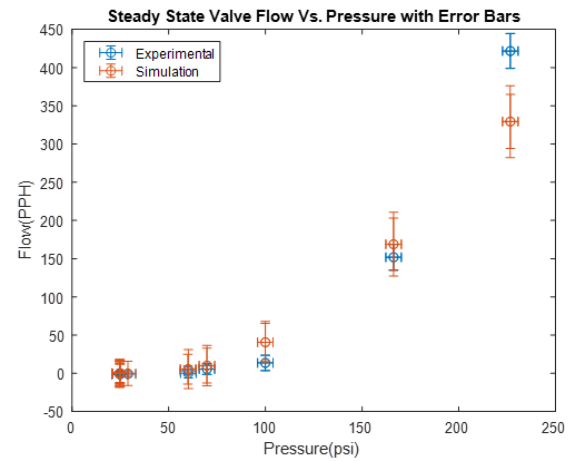


Figure 103: Valve 8 High Impulse Test Program flow

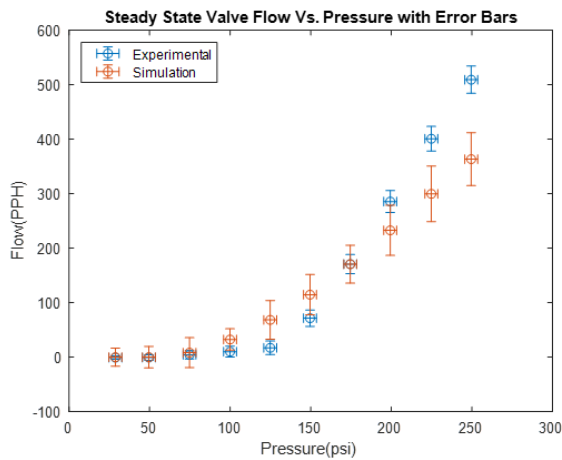


Figure 104: Valve 9 Continuous Step Test Program flow

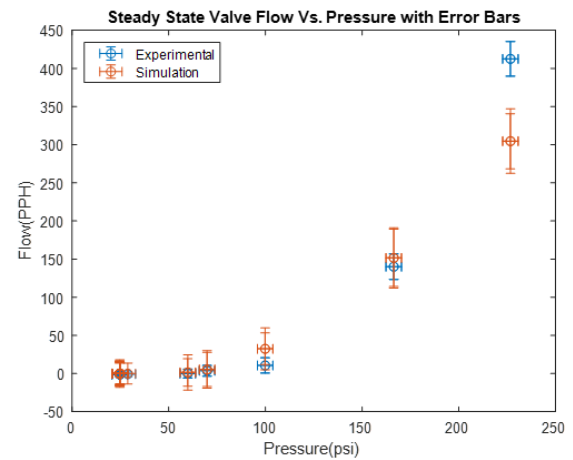


Figure 105: Valve 9 High Impulse Test Program flow

Besides the uncertainty that was accounted for in this research, there were several forms of uncertainty that were not accounted for via quantitative methods. There was also error involved in measuring physical traits that were used for the simulation of each FDV. Even though AATech equipment is calibrated regularly, only a certain degree of accuracy can be achieved with any measurement system. This applies to all geometric features of the valves, geometric data for flow fixtures, spring data, and mass data that was used in the simulation. Besides this, the data collection systems and sensor have an inherent amount of error in their outputs. Due to the number of different empirical data collection methods and instruments, the exact amount of error introduced due to these factors was not easily calculated. It can be assumed though, due to the calibration requirements to meet aerospace standards in a production setting, that the overall effect of these types of error is relatively low.

One of the sources of error in this report was the need to use manual optimization instead of function driven cost analysis optimization. Due to the necessity of visually judging the fit of the simulation outputs to the empirical outputs there is an unknown degree of error in the manually optimized variables.

Another source of an unknown amount of error in the results of this research is the valve slot area calculator that was provided by AATech. Unfortunately, without proving the calculator’s validity in this study the error that calculator introduced to the flow simulation is not known. It is also tough to tell if the calculator was the cause of the simulations poor correlation in regards to the empirical data.

The largest source of error in this research was most likely the interaction of the cavitation and bubbles with the optical sensor. The optical sensor was a primary experimental instrument in the success and failure of this thesis research. The interference in the data collection from cavitation effects was significant. Fig. 106 shows the effect and extent of the optical sensor interference during testing.

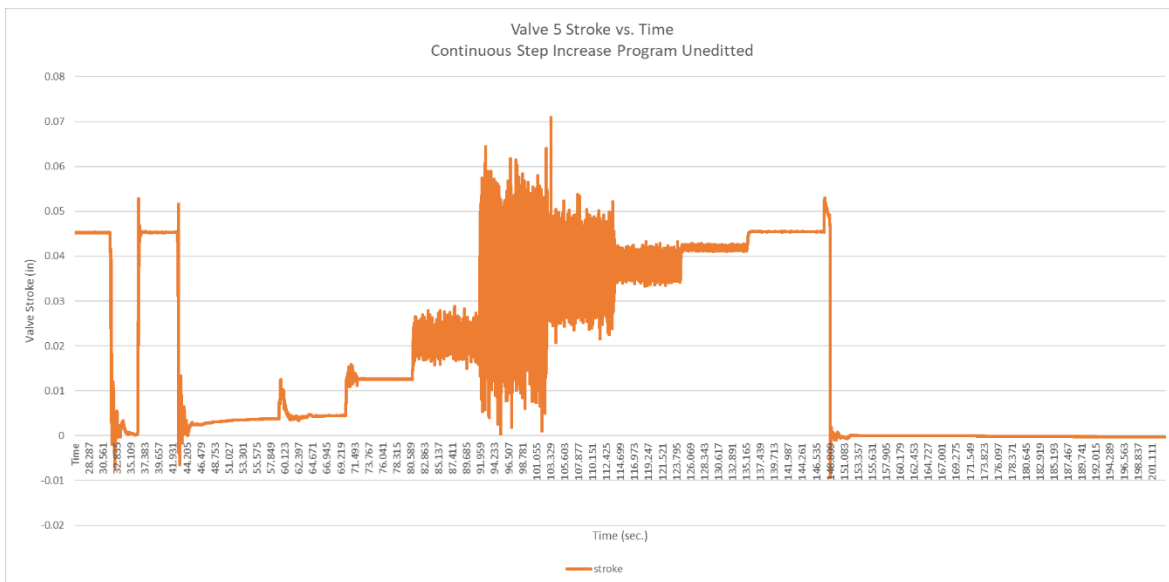


Figure 106: Unprocessed(raw) empirical data of the FDV stroke showing the effects of cavitation.

This figure shows an example of data collected for Valve 5's Continuous Step Increase Program. From 78 seconds to 138 seconds, the valve stroke is impossible to discern.

Even with the majority of the optical sensor interference edited out during the simulation work, there are still examples of the interference. The extent of the interference throughout the testing was too severe to completely eradicate. Fig. 107 and Fig. 108 show enlarged views of the plots from Valve 6 simulation work. In Fig. 107 between 51-54 seconds, you can see an example of the simulation and the experimentally collected valve stroke matching motion exceptionally well. In Fig. 108 between 29-36 seconds there is an example of interference with the experimentally collected stroke data. The simulation behaves as it is expected to in reaction to the pressure differential that is being applied to it. This pressure differential for the simulation comes from the pressure sensors, therefore we can reason that the valve motion shown by the optical sensor is inaccurate. The results in Fig. 108 indicate failure of the stroke measurement, which based on the data available is most likely due to cavitation or bubbles. This type of error had a large impact on this thesis research.

Error was also introduced to the simulation by omitting fluid effects on valve movement as well as other assumptions made in the derivation of the flow number calculations.

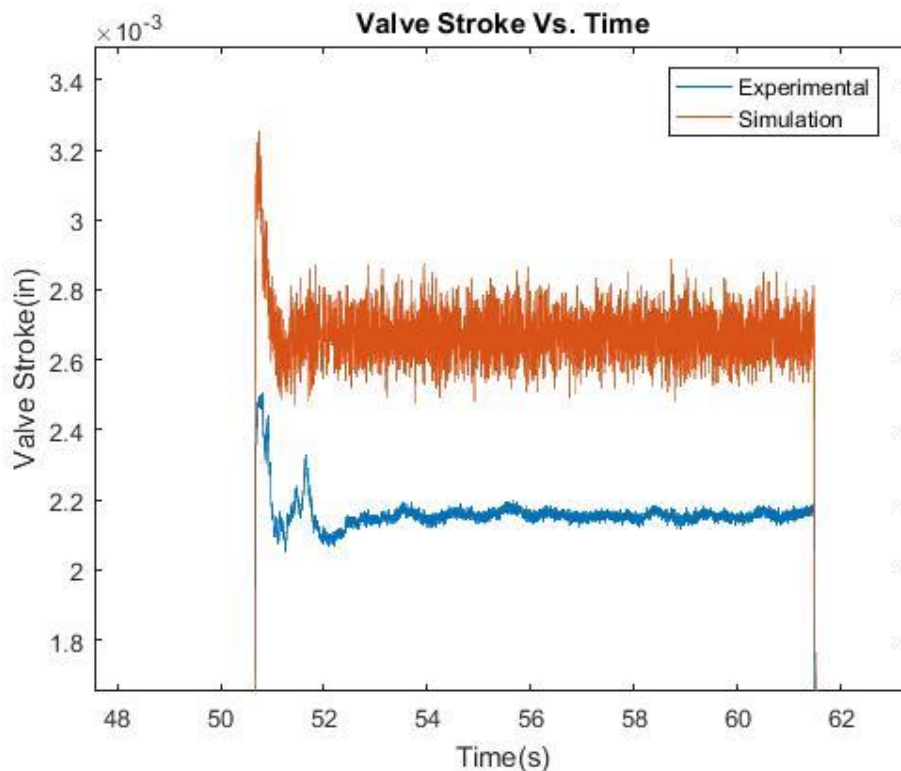


Figure 107: Close up of the simulation of the valve stroke matching well with reality in terms of damped reaction in Valve 6

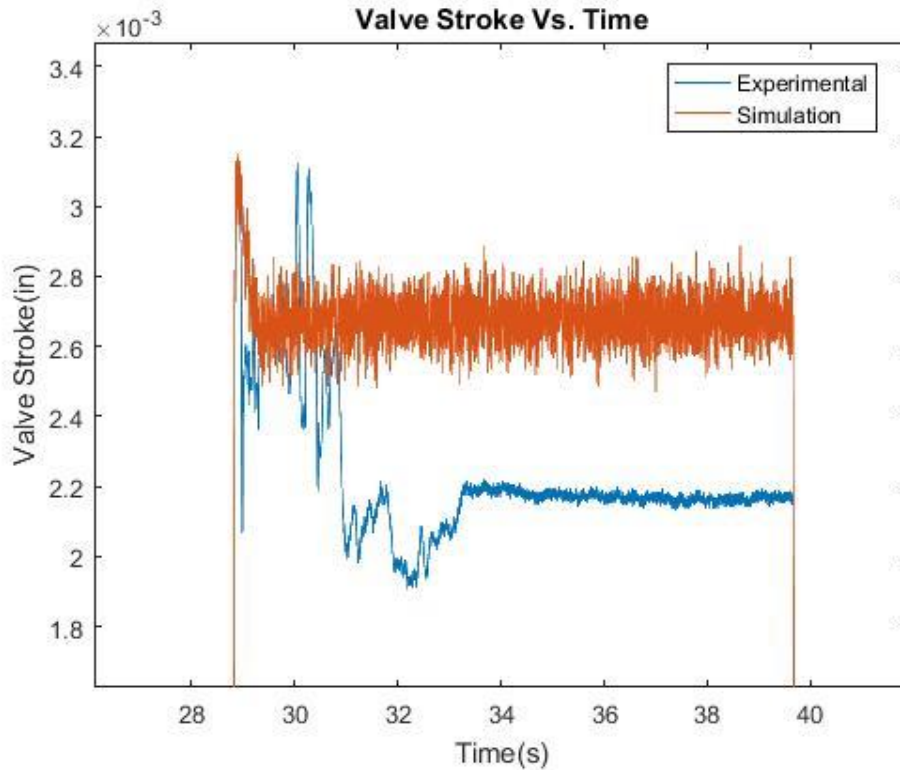


Figure 108: Close up of the simulation of the valve stroke of valve 6 failing to match empirical data due to what appears to be cavitation/bubble interference in the experimental data optical sensor reading.

5.7 Further Research Opportunities

The research presented in this thesis offers numerous opportunities for improvement. The number of unknowns in this research from the accuracy of the FDV flow slot area calculator to the effectiveness of the experimental setup lead to unknown amounts of error, and poor simulation to experimental comparison results.

One large focus for the improvement of research in this specific field should be on the data collection systems. In particular, the Dewesoft system used in this research with the compliment of sensors used was not effective. The optical sensor location and possibly the optical sensor itself was not a satisfactory choice of sensor due to the qualities of the test fluid in motion as well as the effects seen from cavitation and bubbles experienced during pressure drops. It's possible a linear sensor or an optical sensor placed upstream or outside the fixture would have been more effective.

Further development of the simulation could also be considered. More work on the valve area calculation needs to be done to ensure the core calculations in the simulation are accurate. This was a large unknown in this thesis research.

Last, the fluid pressure input programs in which the valves were tested could have been tailored more to reveal characteristics of the valves. If the test stands were capable, then an attempt to instigate a natural frequency response could have been done. This along with all prior mentioned further research should be considered by anyone evaluating similar hardware and experimental techniques.

6. Conclusions

The intent of this thesis research is to generate a computationally simple dynamic valve simulation of aerospace fuel nozzle flow metering check valves for use in industry application where computationally complex solutions might not be an option. This thesis primarily focused on research in the use of a Simulink mass-spring-damper system with augmented MATLAB functions for simulation, the experimental setup with Dewesoft data collection and optical sensor, and the ability to apply cost analysis optimization functions to aerospace fuel nozzle flow metering check valves. The results of the research show that with further development, the experimental data collection is a viable source of high-resolution data. Even with the challenges presented by the optical sensor interference, the system provided high fidelity data in the regions without interference. The results also indicate that the simulation technique is sound but needs further development to meet the needs of a high precision industry such as the aerospace industry. The results of the MATLAB function driven cost analysis based optimization proved to fail in this specific applicable, but could most likely be applied with a small amount of further research. Overall, with some further research into the experimental and simulation techniques this could be a high-quality means of evaluating high precision aerospace fuel nozzle flow metering check valves for industry or research.

7. Bibliography

- [1] H. Xie, J. Liu, H. Yang and X. Fu, "Design of pilot-assisted load control valve for proportional flow control and fast opening performance based on dynamics modeling," *Sensors and Actuators A: Physical*, vol. 235, pp. 95-104, 2015.
- [2] A. L. Knutson, "Modeling and Experimental Valiation of Disc and Reed Style Check Valves fo Hydraulic Applications," Pro Quest LLC, Ann Arbor, 2016.
- [3] B. K. Saha, H. Chattopadhyay, P. B. Mandal and T. Gangopadhyay, "Dynamic simulatio of a pressure regulating and shut-off valve," *Computers & Fluids*, no. 101, pp. 233-240, 2014.
- [4] H. Chattopadhyay, A. Kundu, B. K. Saha and T. Gangopadhyay, "Analysis of flow structure inside a spool type pressure regulating valve," *Energy Conversion and Management*, no. 53, pp. 196-204, 2012.
- [5] E. Frosina, A. Senatore, D. Buono and K. A. Stelson, "A Modeling Approach to Study the Fluid-Dynamic Forces Acting on the Spool of a Flow Control Valve," *Journal of Fluids Engineering*, vol. 139, 2017.
- [6] Y. Ye, C.-B. Yin, X.-D. Li, W.-j. Zhou and F.-f. Yuan, "Effects of groove shape of notch on the flow characteristics of spool valve," *Energy and Conversion Managment*, no. 86, pp. 1091-1101, 2014.
- [7] E. Lisowski and G. Filo, "CFD analysis of the characteristics of a proportional flow control valve with an innovative opening shape," *Energy Conversion and Management*, no. 123, pp. 15-28, 2016.
- [8] E. Leati, C. Gradl and R. Scheidl, "Modeling of a Fast Plate Type Hydraulic Check Valve," *Dynamic Systems, Measurement, and Control*, vol. 138, 2016.
- [9] M.-R. Lee, J.-H. Lee and J.-T. Kim, "Condition Monitoring of a Nuclear Power Plant Check Valve Based on Acoustic Emission and a Neural Network," *Journal of Pressure Vessel Technology*, vol. 127, 2005.
- [10] Q. S. Li, K. Yang, L. Zhang and N. Zhang, "Frequency domain analysis of fluid-structure interaction in liquid filled pipe systems by transfer matrix method," *International Journal of mechanical Sciences*, no. 44, pp. 2067-2087, 2002.
- [11] P. Persson, K. Persson and G. Sandberg, "Reduced order modelling of liquid-filled pipe system," *Journal of Fluids and Structures*, no. 61, pp. 205-217, 2016.
- [12] J. Herrmann, J. Koreck, M. Maess, L. Gaul and O. v. Estorff, "Frequency-dependent damping model for the hydroacoustic finite element analysis of fluid-filled pipes with diameter changes," *Mechanical Systems and Signal Processing*, no. 25, pp. 981-990, 2011.